

63
50

Wavelength Division Multiplexing Technology and Systems

by

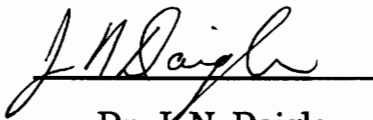
Bindignavile S. Srinivas

Thesis submitted to the Faculty of the
Virginia Polytechnic Institute and State University
in partial fulfillment of the requirements for the degree of
Master of Science
in
Electrical Engineering

APPROVED:



Dr. I. Jacobs, Chairman



Dr. J. N. Daigle



Dr. T. S. Rappaport

May, 1990

Blacksburg, Virginia

LD
5655

V855

1990

S656

C.2

Wavelength Division Multiplexing Technology and Systems

by

Bindignavile S. Srinivas

Dr. Ira Jacobs, Chairman

Electrical Engineering

(ABSTRACT)

Wavelength Division Multiplexed (WDM) based broadband fiber optic networks offer an attractive approach to achieve extremely high throughputs while employing moderate speed electronics. Passive optical filters play a crucial role in such networks serving the function of combining and separating multiple wavelengths. Single and multiple cavity F-P filters are analyzed with particular emphasis on their bandwidth and tuning range. Fabry-Perot (F-P) filter tuning commonly employs piezoelectric techniques. A new tuning technique based on a F-P filter fabricated with a fiber having an electro-optic cladding is proposed. A novel F-P filter structure employing optical feedback is proposed and analyzed. The application of F-P filters in an incoherent multiwavelength star network and the associated concerns involving crosstalk and dispersion are evaluated. A comparative error performance analysis of one and two F-P filter receivers in a BFSK transmission system is performed. An overview of numerous multiwavelength network and switch proposals along with their associated merits and demerits is given.

Acknowledgements

I am grateful to my advisor Dr. Ira Jacobs for his ceaseless encouragement, guidance and motivation during the course of this thesis. The numerous stimulating discussions I have had with him played a major role in helping me complete my thesis.

I would like to thank Dr. J. N. Daigle for his encouragement and goodnatured prodding which kept me going. I wish to extend my appreciation to Dr. T. S. Rappaport for being on my advisory committee.

I would also like to thank Dr. A. Safaai-Jazi and Dr. G. Indebetouw for their guidance and help in the course of this thesis. I sincerely appreciate the help provided by Kent Murphy, Ashish Vengsarkar and R.G. May at various points of my work.

Lastly, I would like to thank AT&T Bell Laboratories for sponsoring this work and FEORC for the material support provided.

Table Of Contents

1.0	Introduction	1
1.1	Optical Filter Technology	2
1.2	Multiwavelength Networks	3
2.0	Optical Filter Technology - A Survey	4
2.1	Fabry-Perot Filters	4
2.2	Diffraction Gratings	6
2.3	Wavelength Selective Directional Couplers	7
3.0	Multiple Cavity Fabry-Perot Filters	10
3.1	Power Transmission Spectrum of the Filter	10
3.2	Tuning Range of the Filter	12
3.3	FWHM Bandwidth of the Filter	13
3.4	Sensitivity to Internal Mirror Reflectivity	14
3.5	Multiple Cavity F-P Filters	15
4.0	Tuning a Fiber Fabry-Perot Filter - A Novel Technique	19
4.1	Principle of the Technique	20

4.2	Discussion	21
5.0	A Novel Fabry-Perot Filter Employing Optical Feedback	22
5.1	Structure of the Filter	22
5.2	Transmission Spectrum of the Filter	23
5.3	FWHM BW Variation with Tap Ratio	24
5.4	Tuning Range of the Filter	25
5.5	Secondary Peak Behavior	26
5.6	Impact of Delay in the Feedback Path	27
5.7	Amplifier in the Forward Path	28
5.8	Conclusion	29
6.0	FDMA M-ary FSK Star Network	31
6.1	Network Architecture	32
6.2	Source Laser Characteristics	33
6.3	Network Crosstalk Power Penalty	33
6.4	Error Performance	38
6.5	Dispersion Penalty	41
6.6	Conclusion	43
7.0	Multiwavelength Packet Switches and Networks	44
7.1	The LAMBDANET Packet Switch	45
7.2	The Photonic Knockout Switch	46
7.3	The FOX Switch	46
7.4	The Shufflenet Packet Switch	47
7.5	The HYPASS Switch	48
7.6	The Bellcore Star-Track Switch	48
7.7	Conclusion	49
8.0	Conclusion	51

9.0	References	72
10.0	Vita	76

List of Illustrations

Figure 1a. A Fiber Fabry-Perot Filter	53
Figure 1b. A GRIN-rod Lens type Littrow Grating	53
Figure 1c. Power transfer characteristics of an Asymmetrical Fiber Coupler	53
Figure 2. Transmission Spectrum of a 3-Mirror F-P with equal reflectivities	54
Figure 3. Transmission Spectra of a 3-Mirror F-P	55
Figure 4. Transmission Spectrum of a 4-Mirror F-P with equal reflectivities	56
Figure 5. Transmission Spectra of a 4-Mirror F-P	57
Figure 6. Transmission Spectrum of a 4-Mirror F-P with unequal reflectivities	58
Figure 7. Improvement in Tuning range in a 3-Mirror F-P	59
Figure 8. Improvement in Tuning range in a 4-Mirror F-P	60
Figure 9. Transmission Spectra of two and multimirror F-P filters	61
Figure 10. Resonant wavelength variation with Δ	62
Figure 11. Geometry of the filter	63
Figure 12. The F-P filter with optical feedback	64
Figure 13. FWHM bandwidth vs. Tap ratio α	65
Figure 14. Transmission Spectrum of the Feedback filter	66
Figure 15. Loss of tuning range improvement in the Feedback filter	67
Figure 16. Improvement in tuning range in the Feedback filter	68
Figure 17. Dependence of Peak transmission and FWHM BW on amplifier gain	69
Figure 18. The FDMA M-ary FSK Star Network	70
Figure 19a. M-ary signal set	71
Figure 19b. Continuous phase M-ary FSK power spectrum	71

List of Tables

Table 1. Performance Parameters and Applications 9

Table 2. Multicavity F-P Filters 18

Table 3. Multiwavelength Packet Switches 50

1.0 Introduction

Wavelength division multiplexing (WDM) technology, by means of which multiple optical signals, each employing a different wavelength, can be simultaneously transmitted over a single optical fiber, is a useful means of exploiting the low-loss characteristics of optical fibers over a broad wavelength region. In addition to an obvious increase in the achievable transmission rate per fiber, WDM systems offer other significant advantages, chief among which are system cost reduction, simultaneous transmission of channels with different bit rates and modulation schemes, and service channel expandability after fiber installation.

The resolving power of conventional optical filters is inadequate to efficiently exploit the huge bandwidth capability of optical fibers. Coherent techniques, in which the sum of the received signal and a locally-generated optical wave is square-law detected, are most efficient, but they impose stringent requirements on laser linewidth and also call for tunable lasers and polarization controllers which result in increased system costs. Consequently there is interest in higher resolution optical filtering techniques that still permit the use of incoherent detection. This thesis focuses on Fabry-Perot filters, considering both the proposal and analysis of new filter structures, as well as the analysis of several system issues.

1.1 Optical Filter Technology

Given the unique characteristics of WDM techniques, its potential applicability in boosting point-to-point transmission capacity is obvious. Additionally, it offers the possibility of employing radically new architectures for future broadband networks both at the network office and subscriber-loop levels. Towards the goal of realizing commercially viable WDM systems, considerable research effort has been directed towards techniques for combining or multiplexing (MUX) multiple wavelengths as well as separating or demultiplexing (DEMUX) them. While a wavelength MUX/DEMUX, henceforth referred to as MULDEM, combines or separates many wavelengths in parallel, wavelength filtering devices (eg. Fabry-Perot filters) select only a single wavelength from an ensemble of wavelengths. A multiplexer is essentially a passive reciprocal device serving as a MUX or a DEMUX in reverse directions.

Prior to launching into an analysis of the operation of fiber Fabry-Perot (FFP) filters and their performance, the reader is presented with an overview of currently employed optical filters and MULDEMs in Chapter 2. This chapter briefly defines and discusses the critical performance parameters of F-P filters, diffraction gratings and wavelength selective directional couplers.

As pointed out earlier, the bulk of this thesis is devoted to the study of the operation and performance of F-P filters. While a single cavity F-P filter is quite impressive in terms of its tuning range, finesse and insertion loss in comparison to the other optical filters, its efficacy as a wavelength selective filter can be greatly boosted by incorporating multiple cavity F-P structures [10]. Chapter 3 analyzes the improvement in bandwidth and tuning range achieved by using multimirror (three and four mirror) structures as well as multicavity F-P filters. The conventional approach employed for tuning a FFP filter involves the piezoelectric stretching of the fiber. Chapter 4 proposes a novel alternative technique for tuning a FFP filter involving the use of an electro-optic cladding.

While Chapter 3 discusses the performance improvement gained by employing multiple (typically two) cavities in tandem, an alternative filter topology, namely the feedback configuration as proposed by us, is also feasible. In Chapter 5, a novel F-P filter employing optical feedback is proposed and analyzed. The chapter also describes the inherent shortcomings of the filter as well as techniques to overcome them.

1.2 Multiwavelength Networks

After the first five chapters of the thesis, the reader will be adequately equipped with a knowledge of the principle of operation and the performance of F-P filters including several new means for enhancing their performance. The next two chapters discuss the application of F-P filters in practical situations. Chapter 6 describes an incoherent multiwavelength star network employing M-ary FSK modulation with FFP filters as wavelength demultiplexers. The chapter also discusses associated concerns including source laser performance requirements and system crosstalk power penalties. The concluding sections of this chapter analyze the performance of a two filter receiver versus that of a single filter one in an incoherent binary frequency shift keying (BFSK) modulation based network, and the impact of dispersion in the same network.

The two major strengths of optical fiber technology, namely its inherent broadcast structure (using star couplers) as well as the huge bandwidth of the fiber, have been exploited in numerous multiwavelength photonic switch and network proposals. Chapter 7 surveys six different proposals that have appeared in the literature and discusses their merits and demerits. Chapter 8 summarizes the principal results of this thesis.

2.0 Optical Filter Technology - A Survey

As was indicated in the introductory chapter, optical filters and MULDEMs are passive devices. As such, they provide a simple and economical way of combining (MUX) multiple wavelengths at the transmitting end as well as separating (DEMUX) them at the receiving end. This chapter describes the behavior of three different filtering and multiplexing technologies namely the Fabry-Perot (F-P) filter, the diffraction grating and the wavelength selective directional coupler. It must be emphasized that the term *multiplexing* is reserved for technologies that can combine and separate multiple wavelengths in parallel whereas *filtering* devices select only a single wavelength from an ensemble of wavelengths.

2.1 *Fabry-Perot Filters*

A Fabry-Perot (F-P) filter works on the principle of multiple partial reflections within a cavity to produce peaks and nulls in the frequency domain. It consists essentially of a resonant cavity formed by a parallel pair of highly reflective end faces with the separation being very large compared to the wavelength (see Fig. 1a). Owing to considerations of compactness and since the F-P filter is a single transverse mode device, single-mode fiber based filters have been proposed and constructed. While studying the applicability of F-P filters for selecting a particular channel from an ensemble of wavelengths, the primary performance

parameters to be considered are the filter's finesse (to be defined below), the tuning range (also called the Free Spectral Range or FSR) and the insertion loss. The periodic power transmission spectrum of an ideal F-P filter is given by the well known Airy's equation [1],

$$T(f) = \frac{1}{1 + \left(\frac{2F}{\pi}\right)^2 \sin^2\left(\frac{\pi f}{\text{FSR}}\right)} \quad (2.1.1)$$

where 'f' is the frequency deviation from a resonant peak of the F-P cavity. The finesse (F) is defined as the ratio of the FSR to the FWHM (full width half maximum or the 3 dB bandwidth) bandwidth of the filter where both FSR and FWHM are expressed in frequency or wavelength terms. The reflection finesse (F_R) is given by

$$F_R = \frac{\pi}{2 \cdot \arcsin\left[\frac{1-R}{2\sqrt{R}}\right]}$$

where R is the reflectivity of the end mirrors. It is readily shown that when R is close to unity, the filter's reflection finesse is approximated by

$$F_R = \frac{\pi\sqrt{R}}{1-R} \quad (2.1.2)$$

The finesse, F, is actually less than the reflection finesse F_R due to defects that may be present in the filter such as fiber-mirror gap, finite mirror thickness, mirror-tilt loss and endface curvature loss.

Researchers have reported the successful fabrication of ultrahigh finesse F-P filters operating at 1.52 μm with F of the order of 500 and with insertion loss of 4 to 5 dB [2]. The FWHM bandwidth of this filter was reported as being below 1 MHz ($\Delta\lambda = 0.01\text{pm}$). Moderate finesse filters (F upto 200) having insertion loss as low as 1.5 dB have also been reported [3].

The tuning range of the F-P filter is limited to its free spectral range (FSR) which is the wavelength spacing between the transmission peaks of the resonant cavity and is given by (in wavelength terms)

$$\text{FSR} = \frac{\lambda^2}{2nL} \quad (2.1.3)$$

where n is the effective index of refraction and L is the cavity length. As is evident from (2.1.3), the FSR

can be increased by decreasing L . However, increasing the FSR generally results in an increased bandwidth (BW) as the fabrication of extremely high reflectivity mirrors to achieve higher values of F becomes increasingly more difficult.

F-P filters may be tuned over the FSR by stretching the fiber using piezoelectric techniques. Alternatively, we have considered the use of a fiber having an electro-optic cladding such that the cladding index may be varied while holding the phase constant fixed. The details of this are discussed in Chapter 4.

F-P filters are primarily employed in optical FDM based systems having channel spacings of the order of 0.1 nm owing to their very high resolution powers. Since they are based on the principle of filtering out a single wavelength, they are mainly employed in an architecture using the split and filter technique. This implies a $1/N$ splitting loss which might limit the number of channels/users the system can support. Hence, while it is inefficient for applications requiring simultaneous access to all channels (eg. central office), it would be highly suitable for installation at subscriber premises where access to a single or a small subset of channels is required.

2.2 *Diffraction Gratings*

Diffraction gratings provide an inherently parallel structure to achieve multi-channel multiplexing or demultiplexing. The Littrow type grating [4], which is the most extensively studied grating structure, has the following principle of operation considering its application as a DEMUX (demultiplexer). When the wavelength multiplexed light from the input fiber is incident on the grating (after being collimated by a lens), at an angle of incidence θ_i , different wavelength components are diffracted at different angles θ in accordance with the grating equation [5]

$$m\lambda = d(\sin\theta - \sin\theta_i) \quad (2.2.1)$$

where m is the grating order. The individual wavelengths are then refocused to a different spot on the output fiber array arranged in the focal plane of the lens (see Fig. 1b). As is evident, the grating has a multiplicity of passbands associated with the multiple output ports.

The unambiguous wavelength operating range (i.e., without overlap) of a grating is called its free

spectral range (FSR) and is given by

$$\text{FSR} = \frac{\lambda}{m} \quad (2.2.2)$$

To minimize insertion loss, gratings are generally employed with multimode output fibers and single mode input fibers which make them more useful as DEMUXes rather than as MUXes. Commercially available grating-based MULDEMs have achieved crosstalk levels on the order of -30 dB with insertion losses from 1 to 7 dB [6]. Channel spacings on the order of 1 to 2 nm, while accommodating over 20 channels have been achieved. Even larger numbers of channels (40 to 50) are expected to be accommodated in the near future. Bandwidths in the range of 0.1 nm have been realized.

Grating based devices are commonly employed in order to combine or separate many channels in parallel. Hence, they are prime candidates for use at network endpoints where simultaneous access to all channels is required. It must be noted that grating structures as discussed here are essentially untunable and hence are unfit for architectures employing dynamic channel assignment. However, a limited tunability has been achieved [7] by varying the spatial period of the grating as seen by the evanescent field in a fiber.

2.3 Wavelength Selective Directional Couplers

Single-mode directional couplers are inherently wavelength sensitive. This is evident from the fact that the coupling ratio is a sinusoidal function of the coupling strength (c) which in turn is approximately inversely proportional to wavelength [8]. Hence, by making c sufficiently large, it is possible to ensure that the coupling strength is near unity at one wavelength and near zero at another. True bandpass characteristics are obtained in asymmetrical couplers made from dissimilar fibers (different core diameters and refractive index differences between core and cladding) as seen in Fig. 1c. The coupler's FWHM bandwidth is a strong function of the effective index difference change with wavelength as well as the interaction length. Hence, in order to achieve a narrow bandwidth without requiring a large interaction length, the intersection angle of the β - dispersion curves (the curves representing the dependence of the phase constant β on the wavelength for each fiber) must be increased. Increasing the radii of curvature of the fibers also helps in reducing the bandwidth. To achieve high coupling efficiency at the crossover

wavelength, the core spacing and the length of the coupling region must be carefully chosen.

An asymmetric fiber coupler with an FWHM bandwidth of 22.5 nm, a maximum sidelobe level of -11 dB and an insertion loss of 0.5 dB has been reported [9]. Asymmetric couplers made from electro-optic waveguides (eg. Ti:LiNbO₃) afford a limited amount of tunability.

Owing to their wide passbands, asymmetric couplers are well-suited for the separation of only two widely separated channels. In principle, multiple channels can be demultiplexed using a hierarchy of couplers in a tree-like fashion but the associated insertion loss and crosstalk degradation precludes this possibility.

Table 1 provides an overview of the principal performance parameters of the three optical filters/MUXes discussed in this chapter and includes their fields of application. Note that the term *optical frequency division multiplexing* (Optical FDM) seen in Table 1 is used for resolutions less than about 0.1 nm (corresponding to frequency channel spacings less than about 12.5 GHz at 1.55 μm) while *wavelength division multiplexing* (WDM) is used for resolutions of the order of 1.0 nm and higher.

Table - 1

Performance Parameters and Applications

	FWHM BW	FINESSE	TUNABILITY	INSERTION LOSS	APPLICATIONS
I	~ 0.1 nm	High	High	~ 1 dB	Optical FDM
II	~ 1.0 nm	Moderate	Limited	~ 4 dB	Dense WDM
III	~ 10 nm	-	None	~ 0.5 dB	Coarse WDM

where,

- I** - Fabry-Perot Filter
- II** - Diffraction Grating
- III** - Wavelength Selective Directional Coupler

3.0 Multiple Cavity Fabry-Perot Filters

In the previous chapter we described the behaviour and the critical performance parameters of three different filtering technologies. The efficacy of a F-P filter as a wavelength selective filter can be significantly improved by employing multiple cavity structures. This chapter details the study of multimirror and multicavity (separate cavities) F-P structures with particular attention being paid to filter bandwidth and tuning range improvement as well as to issues of sensitivity. Rather than partitioning the chapter into individual sections dealing with three and four mirror structures respectively, a comparative approach has been employed. The final section of the chapter analyzes multicavity filters.

3.1 Power Transmission Spectrum Of The Filter

The power transmission spectrum of a three mirror F-P filter is given by [10]

$$T(f) = \frac{(1-R_1)(1-R_2)(1-R_3)}{|1 - \sqrt{R_1 R_2} \exp(-j2\phi_1) - \sqrt{R_2 R_3} \exp(-j2\phi_2) + \sqrt{R_1 R_3} \exp(-j2(\phi_1 + \phi_2))|^2} \quad (3.1.1)$$

where R_1, R_3 = end mirror reflectivities,
 R_2 = central mirror reflectivity,
 f = frequency offset from common resonance frequency of both cavities,

FSR_i = Free Spectral Range of the i^{th} cavity,

$$\text{and } \phi_i = (\pi f)/FSR_i, i = 1, 2$$

The three mirrors are placed parallel to each other with the lengths of the two resultant cavities being possibly different. The expression (3.1.1) is easily derived by using boundary condition techniques (i.e., electric field continuity at the boundary) at the three mirrors. As is evident from Fig. 2, a filter with equal mirror reflectivities for all the three mirrors is an undesirable structure owing to the occurrence of ripples in the transmission spectrum. The transmission curves for various values of the central mirror reflectivity are shown in Fig. 3. It may be noted that the filter displays a ripple free curve with unity peak transmission only for a certain critical value of central mirror reflectivity given by [10],

$$R_{2,c} = \left(\frac{\sqrt{R_1} + \sqrt{R_3}}{1 + \sqrt{R_1 R_3}} \right)^2 \quad (3.1.2)$$

This result can be easily proved by setting T to unity at a resonant frequency for both cavities (i.e., $\phi_1 = \phi_2 = 0$). We will return to Fig. 3 for further comments in a later section of this chapter.

Turning our attention to the four mirror filter, its power transmission is given [11] by an expression similar to (3.1.1). As seen in Fig. 4, one may note that the power transmission spectrum of the filter displays ripples in its passband for equal mirror reflectivities. The filter displays a ripple free unity peak transmission curve (refer Fig. 5) for structures with inner mirror reflectivities being equal and above a certain critical value given implicitly by the relation [11]

$$R_2 + \sqrt{\frac{R_2}{R_1}} (1 + R_1) = 3 \quad (3.1.3)$$

As indicated above, this spectrum is observed only for a symmetrical filter structure with $R_1 = R_4$ and $R_2 = R_3$. Asymmetrical structures with unequal mirror reflectivities result in undesirable transmission spectra displaying ripples in the passband and peak transmission significantly smaller than unity as seen in Fig. 6. Thus, four mirror filters display a behavior markedly different from their three mirror counterparts as far as asymmetry is concerned. Hence, we conclude that symmetry is a desirable characteristic in four mirror F-P filters.

3.2 Tuning Range Of The Filter

This section concentrates on the significant improvement in tuning range achievable by employing multiple mirror F-P structures. However, this improvement may be realized only by employing cavities with slightly different free spectral ranges (FSR's) thus taking advantage of the vernier effect. The improvement is achieved by virtue of the fact that only those frequencies which are simultaneously resonant in all the cavities are transmitted with near zero attenuation.

Considering the three mirror structure, the equivalent FSR of the filter is given by [10]

$$FSR_{eq} = \frac{FSR_1 \cdot FSR_2}{|FSR_2 - FSR_1|} \quad (3.2.1)$$

A eleven fold improvement in tuning range may be realized by using a three mirror structure as seen in Fig. 7. This curve has been generated using (3.1.1). As is evident, the increase in FSR is in agreement with that obtained from (3.2.1).

Shifting our attention to the four mirror structure, we may determine the equivalent FSR of the filter as discussed below. Let FSR_1 , FSR_2 and FSR_3 be the three free spectral ranges of the three cavities with the added assumption that $FSR_1 < FSR_2 < FSR_3$. Additionally, the FSR's are only slightly different from each other to take advantage of the vernier effect. Further, let

$$\Delta_{12} = FSR_2 - FSR_1 \quad (3.2.2)$$

$$\Delta_{23} = FSR_3 - FSR_2 \quad (3.2.3)$$

Now, considering cavities 1 and 2, from (3.2.1) we get

$$FSR_{1eq} = \frac{FSR_1 \cdot FSR_2}{\Delta_{12}} \quad (3.2.4)$$

Similarly, considering cavities 2 and 3, we get

$$FSR_{2eq} = \frac{FSR_2 \cdot FSR_3}{\Delta_{23}} \quad (3.2.5)$$

Let,

$$FSR = \max(FSR_{1eq}, FSR_{2eq}) \quad (3.2.6)$$

Finally, assuming a hypothetical two cavity filter with tuning ranges of FSR_{1eq} and FSR_{2eq} respectively and following the same approach as employed earlier, we conclude that the equivalent tuning range of the three cavity filter is

$$FSR_{eq} = c.FSR \quad (3.2.7)$$

where

$$c = \frac{\min (FSR_{1eq}, FSR_{2eq})}{|FSR_{2eq} - FSR_{1eq}|} , \quad c \in I \quad (3.2.8)$$

Again, a fifteen fold improvement in tuning range can be achieved by using a four mirror structure as seen in Fig. 8. This curve has been generated using the power transmission spectrum equation for a four mirror filter [11]. As is evident, this is in agreement with (3.2.7).

3.3 FWHM Bandwidth Of The Filter

The power transmission spectrum of the three mirror filter, with the central mirror having a critical reflectivity value, end mirrors having equal reflectivities and with the two tuning ranges being equal, is (as derived from (3.1.1)) [11]

$$T(f) = \left[1 + \left(\frac{16R(1+R)^2}{(1-R)^4} \right) \sin^4 \left(\frac{\pi f}{FSR} \right) \right]^{-1} \quad (3.3.1)$$

where R is the reflectivity of the end mirrors. For large R, the FWHM bandwidth of the filter can easily be obtained as

$$FWHM_3 \approx \frac{1-R}{\sqrt{2R}} \approx \frac{FWHM_2}{\sqrt{2}} \quad (3.3.2)$$

where the subscripts represent the number of mirrors in the filter.

In an analogous manner, the transmission spectrum of a four mirror filter, under conditions similar to those assumed for the three mirror filter, is expressed as [11]

$$T(f) = \left[1 + \left(\frac{64R_1}{(1-R_1)^2(1-R_2)^2} \right) \sin^6 \left(\frac{\pi f}{\text{FSR}} \right) \right]^{-1} \quad (3.3.3)$$

where R_1 and R_2 are the reflectivities of the inner and outer mirrors respectively. For large reflectivities, the FWHM bandwidth of the four mirror filter is given by

$$\text{FWHM}_4 \approx \left[\frac{(1-R_1)^2(1-R_2)^2}{R_1} \right]^{1/6} \approx \frac{\text{FWHM}_2}{2} \quad (3.3.4)$$

Thus, employing multiple mirror structures results in a significant increase in the tuning range of the filter as well as a decrease in its FWHM bandwidth thus enabling the achievement of extremely high finesses. Also, while the effective passband transmission through the two mirror filter cuts off as f^{-2} , it cuts off as f^{-4} and f^{-6} in three and four mirror filters respectively as seen in Fig. 9. The multimirror filters have flatter passband responses too.

3.4 Sensitivity To Internal Mirror Reflectivity

To begin with, we investigated the sensitivity of the transmission of the three mirror filter at band center with respect to the central mirror's reflectivity. From (3.1.1), the transmission of the three mirror filter at the band center is given by

$$T(0) = \frac{(1-R_1)(1-R_2)(1-R_3)}{|1 - \sqrt{R_1 R_2} - \sqrt{R_2 R_3} + \sqrt{R_1 R_3}|^2} \quad (3.4.1)$$

The critical reflectivity of the central mirror given by (3.1.2) can be expressed in terms of its transmissivity ($\tau = 1 - R$) as [10]

$$\tau_{2,c} = \frac{\tau_1 \cdot \tau_3}{4} \quad (3.4.2)$$

The central mirror's transmissivity can now be expressed in terms of its critical value as $\tau = \eta \tau_{2,c}$, where η is the deviation from the critical value. Hence, the transmission of the three mirror filter at the

band center is given by

$$\therefore T(0) \approx \frac{4\eta}{(1+\eta)^2} \quad (3.4.3)$$

As may be noted from (3.4.3), a 10% variation in transmissivity ($\eta=0.9$) results in a 0.28% decrease in the peak transmission of the three mirror filter. Turning our attention to the four mirror filter, the filter's transmission at band center when the outer and inner mirrors have equal reflectivities in pairs is

$$T(0) = 1 \quad (3.4.4)$$

This result is significant since it shows that the four mirror filter is less sensitive to internal mirror reflectivity variations in comparison to that in the three mirror filter assuming that symmetry is maintained. However, while the four mirror filter's transmission at band center remains unaltered as seen from (3.4.4), the filter's bandwidth decreases as shown in Fig. 5. Also, for filters with mirror reflectivities less than the critical value, the transmission spectrum has ripples in the passband as seen in Fig. 5.

3.5 *Multiple Cavity F-P Filters*

While the preceding sections deal with multiple mirror F-P filters, this section concentrates on multicavity filters which display a significant improvement in filter performance in terms of filter bandwidth as well as tuning range. However, since multicavity F-P structures have separate cavities, care must be taken to suppress the distortion caused by intercavity resonances. Two of the most commonly employed techniques to achieve the same are the use of an isolator between the two cavities or alternatively, the separation of the cavities by a length of fiber (L) greater than the coherence length of the signal transmitted by the first F-P cavity (L_C) [10]. The isolator suppresses the reflected power while the second technique ensures that the forward and reflected fields are incoherent and thus the interfilter cavity does not resonate. The FSR of the two cavity structures in both the cases is given by (3.2.1).

Assuming that the power transmission spectrum of a single F-P cavity can be closely approximated by

$$T(f) \approx \left[1 + \left(\frac{2f}{W} \right)^2 \right]^{-1} \quad , \quad |f| < W \ll \text{FSR} \quad (3.5.1)$$

$$\approx \left(\frac{W}{2f} \right)^2 \quad , \quad W < |f| \ll \text{FSR}$$

where W is the FWHM bandwidth of the filter, the transmission spectrum of a two cavity filter using an isolator is given by (assuming identical cavity bandwidths and simultaneous resonance at $f=0$)

$$T(f) \approx \left[1 + \left(\frac{2f}{W} \right)^2 \right]^{-2} \quad , \quad |f| < W < \text{FSR}_1, \text{FSR}_2 \quad (3.5.2)$$

$$\approx \left(\frac{W}{2f} \right)^4 \quad , \quad W < |f| \ll \text{FSR}_1, \text{FSR}_2$$

and that of a two cavity filter with the cavities separated by a length greater than the coherence length is

$$T(f) \approx \left[1 + 2 \left(\frac{2f}{W} \right)^2 \right]^{-1} \quad , \quad |f| < W \ll \text{FSR}_1, \text{FSR}_2 \quad (3.5.3)$$

$$\approx \frac{1}{2} \left(\frac{W}{2f} \right)^2 \quad , \quad W < |f| \ll \text{FSR}_1, \text{FSR}_2$$

which is obtained by tracking the multiple reflections and adding them on a power basis rather than on an electric-field basis since the reflections add incoherently [10]. In other words, (3.5.3) is derived by taking the statistical average of the magnitude squared of the sum of the complex electric-field vectors assumed to have random phases.

The corresponding FWHM bandwidths of the two filters are

$$\text{FWHM} = [\sqrt{2} - 1]^{1/2} \cdot W \quad (\text{Isolator}) \quad (3.5.4)$$

$$\text{FWHM} = \frac{W}{\sqrt{2}} \quad (L) \gg L_C \quad (3.5.5)$$

Table 2 gives a brief summary of the transmission spectra and the FWHM bandwidths of the filters discussed in this chapter. It is seen from Table 2 that as the number of mirrors (or cavities) increases the filter passband falls off more rapidly. Additionally, the filter FWHM bandwidth also decreases by a factor of

$\sqrt{2}$ for every additional mirror in the filter structure. The two cavity filter (feedback) entry in Table 2 corresponds to a structure considered in Chapter 5.

Table - 2
Multicavity F-P Filters

	T(f)	FWHM
2 Mirror Filter	$\left[1 + \left(\frac{2f}{W}\right)^2\right]^{-1}$	$W \approx \frac{1-R}{\sqrt{R}}$
3 Mirror Filter	$\left[1+4\left(\frac{2f}{W}\right)^4\right]^{-1}$	$\frac{W}{\sqrt{2}}$
4 Mirror Filter	$\left[1+64\left(\frac{2f}{W}\right)^6\right]^{-1}$	$\frac{W}{2}$
2 Cavity Filter ($L > L_c$)	$\left[1+2\left(\frac{2f}{W}\right)^2\right]^{-1}$	$\frac{W}{\sqrt{2}}$
2 Cavity Filter (Feedback)	$\frac{(1-\alpha)^2 \cdot \left[1 + \left(\frac{2f}{W}\right)^2\right]}{\left[1 + \left(\frac{2f}{W}\right)^2\right]^2 - \alpha^2}$	$\sqrt{(\sqrt{1-\alpha^2+\alpha^4} - \alpha^2)} W$
2 Cavity Filter (Isolator)	$\left[1 + \left(\frac{2f}{W}\right)^2\right]^{-2}$	$[\sqrt{2} - 1]^{1/2} \cdot W$

W = FWHM BW of a single cavity F-P filter and α = Tap ratio of the directional couplers.

4.0 Tuning A Fiber Fabry-Perot Filter - A Novel Technique

Fiber Fabry-Perot (FFP) filters have an important role to play in fiber based star networks employing fine WDM to provide network access to a multiplicity of users. Instead of using heterodyning techniques requiring costly tunable and highly stable local oscillators as well as polarization controllers, tunable FFP filters can be employed at the cost of a poorer receiver sensitivity than may be achieved with coherent techniques. However, it must be pointed out that optical filtering followed by an optical amplifier and an incoherent detector can result in receiver sensitivities close to the best achievable by coherent techniques. In the previous chapters, the principal performance parameters of a F-P filter were defined as well as the improvement in wavelength selectivity achieved by using multiple mirror F-P structures were analyzed. The FFP filter considered here employs a single mode fiber with an extremely thin cladding so as to ensure that the cladding index of refraction (that of the liquid crystal cladding) is electrically alterable.

The conventional technique for tuning a FFP filter essentially involves altering the optical path length of the fiber. This is achieved by piezoelectrically stretching the fiber so as to achieve a resonant length at the desired wavelength. In this chapter, we suggest an alternative strategy for tuning the filter which involves altering the index of refraction of the cladding.

4.1 Principle Of The Technique

In a F-P filter, it can be shown that the condition for resonance for normal incidence is

$$\beta d = m\pi \quad (4.1.1)$$

where β is the phase constant. Over one free spectral range (FSR) of the F-P filter, the order number m is a constant. Since our technique does not employ stress tuning, the length d of the fiber is also a fixed parameter. Thus, in order to tune the filter over one FSR, the phase constant β must be maintained constant over the wavelength range of one FSR. The phase constant is related to the wavelength λ by the relation [12]

$$\beta = \frac{2\pi n_1}{\lambda} \cdot (1 + \Delta b) \quad (4.1.2)$$

where n_1 is the index of refraction of the core, b is the normalized propagation constant and Δ is given by

$$\Delta = \frac{n_1 - n_2}{n_1} \quad (4.1.3)$$

where n_2 is the cladding index.

Thus, to maintain β constant over the wavelength range of one FSR, we suggest varying the parameter Δ . In other words, altering the refractive index of the cladding can serve to tune the filter. However, it must be realized that the normalized propagation constant b is a function of Δ and λ . The normalized frequency V of operation is given by

$$V = \frac{2\pi a}{\lambda} \cdot (n_1^2 - n_2^2)^{1/2} \approx \frac{2\pi a n_1}{\lambda} \cdot \sqrt{2\Delta} \quad (4.1.4)$$

For all practical purposes, one may assume that V is independent of λ and is dependent on Δ only over one FSR. Besides, considering the FSR of the filter (~ 10 nm), the wavelength dependence of the refractive index of the core has been ignored. In order to determine b at different wavelengths, we solved the characteristic equation for the LP_{01} mode [12] given by

$$\frac{uJ_1(u)}{J_0(u)} - \frac{wK_1(w)}{K_0(w)} = 0 \quad (4.1.5)$$

where

$$u^2 + w^2 = V^2 \quad (4.1.6)$$

Also

$$b = 1 - \frac{u^2}{V^2} \quad (4.1.7)$$

In (4.1.5), J_1 and J_0 are the Bessel functions of the first kind, K_1 and K_0 are the modified Bessel functions of the second kind and u and w are the normalized propagation constants in the core and cladding respectively.

The characteristic equation was solved using numerical techniques. The computation was carried out for a FFP filter with core radius of 4 μm , nominal wavelength 1550 nm and Δ varying over a range of 0.001 to 0.005. Variation in Δ was restricted to this range to ensure single mode operation ($V < 2.405$). The dependence of the resonance wavelength on Δ is shown in Fig. 10.

4.2 Discussion

As can be noted from Fig. 10, by varying Δ over the range 0.001 to 0.005 (so as to ensure the single mode regime of operation), the resonant wavelength of the F-P filter (or equivalently, the wavelength for which the phase constant β is unchanged) varies over a range of 4 nm. (1550 to 1554 nm). Also, Δ is not lowered too much to ensure that the LP_{01} mode is not completely radiated away (i.e., V must not be too low). Thus, varying the cladding index to tune the filter is feasible. In order to achieve refractive index variation in the cladding, we suggest using electro-optic materials. However, to ensure low voltage operation, a material with a high electro-optic coefficient would be desirable as a cladding. We suggest the use of liquid crystals to serve as a cladding. For example, MBBA, a liquid crystal, has a critical voltage of only 4.2 V [13] (voltages above the critical voltage are needed to achieve a change in the refractive index). The geometry of an exemplary filter is shown in Fig. 11.

5.0 A Novel Fabry-Perot Filter Employing Optical Feedback

Fabry-Perot [F-P] filters employing two cavities in tandem have been reported in numerous papers [10], [11] and are discussed in Chapter 3. The tandem structure improves the tuning range and the FWHM bandwidth significantly. In this chapter, a novel F-P filter using two cavities, not in tandem, but in a feedback topology is proposed and analyzed. A patent disclosure on this proposal was submitted to VTIP on February 28, 1990. The improvement to be gained in tuning range and FWHM bandwidth over that of a single F-P cavity are also reported here.

5.1 *Structure Of The Filter*

As may be noted in Fig. 12, the proposed filter consists of two F-P cavities with one cavity forming the forward path and the other the feedback path. Optical taps for the feedback path are provided by employing identical directional couplers at the two ends. Each cavity is assumed to be symmetrical or in other words, the end face reflectivities are equal.

5.2 Transmission Spectrum Of The Filter

Referring to Fig. 12, we define the following terms,

$G(f)$ = transmission spectrum of cavity 1

$H(f)$ = transmission spectrum of cavity 2

α = tap ratio of both directional couplers

R_1 = mirror reflectivities of cavity 1

R_2 = mirror reflectivities of cavity 2

FSR_i = free spectral range of cavity 'i', $i = 1, 2$

f = frequency offset from common resonance frequency of both cavities

The transmission spectra of the individual cavities, assuming that they are ideal, are (from (2.1.1))

$$G(f) = \frac{1}{1 + \frac{4R_1}{(1 - R_1)^2} \sin^2\left(\frac{\pi f}{FSR_1}\right)} \quad (5.2.1)$$

$$H(f) = \frac{1}{1 + \frac{4R_2}{(1 - R_2)^2} \sin^2\left(\frac{\pi f}{FSR_2}\right)} \quad (5.2.2)$$

Let $X(f)$ be the normalized output power of cavity 1 (see Fig.12). Also, let $Y(f)$ be the normalized output power of the filter (i.e. on the output side of the directional coupler on the right)

$$X(f) = G(f) \left[(1-\alpha) + \alpha^2 H(f) X(f) \right] \quad (5.2.3)$$

$$\therefore X(f) = \frac{(1-\alpha)G(f)}{1-\alpha^2 G(f)H(f)} \quad (5.2.4)$$

Hence,

$$T(f) = \frac{Y(f)}{1} = X(f) \cdot (1-\alpha) = \frac{G(f) \cdot (1-\alpha)^2}{1-\alpha^2 G(f) \cdot H(f)} \quad (5.2.5)$$

This result has been derived on the assumption that the cavities are separated by a length of fiber greater than the coherence length of the source being used. This is done to suppress the intercavity resonances which cause distortion. However, this introduces a differential delay that modifies the frequency response. This effect will be considered in Section 5.6. Also, note that the peak transmission of the filter is [with $G(0) = H(0) = 1$]

$$T(0) = \frac{1-\alpha}{1+\alpha} < 1 \quad (5.2.6)$$

Hence, in order to maximize the peak transmission of the filter, the tap ratio α of the couplers must be made small. We will now investigate the sensitivity of the transmission spectrum to variation in α .

5.3 FWHM BW Variation With Tap Ratio

Assuming that the FWHM bandwidths of the two cavities are identical ($W = FSR_1/F_1 = FSR_2/F_2$), the transmission spectra of the cavities in the vicinity of the resonance may be expressed as (from 3.5.1)

$$G(f) = H(f) \approx \frac{1}{1 + \left(\frac{2f}{W}\right)^2}, \quad |f| < W \ll FSR_1, FSR_2 \quad (5.3.1)$$

Hence, the transmission spectrum of the filter may be expressed as,

$$T(f) \approx \frac{(1-\alpha)^2 \left[1 + \left(\frac{2f}{W}\right)^2\right]}{\left[1 + \left(\frac{2f}{W}\right)^2\right]^2 - \alpha^2} \quad (5.3.2)$$

In order to obtain the FWHM bandwidth of the filter, putting $T(\text{FWHM}/2) = (1/2) \cdot T(0)$, we conclude

that,

$$\text{FWHM} = \left[\sqrt{1 - \alpha^2 + \alpha^4} - \alpha^2 \right]^{1/2} \cdot W \quad (5.3.3)$$

As may be noted from (5.3.3) as well as Fig. 13, the FWHM bandwidth of the filter decreases as the tap ratio α increases. This decrease in bandwidth is also noted in Fig. 14 where the response is shown for two values of α . Additionally, Fig. 14 confirms the decrease in bandwidth achievable over that of a single F-P cavity when the proposed structure is employed. However, as pointed out in an earlier section, an increase in α also causes a decrease in peak transmission as seen in Fig. 14. Using (5.2.6) and (5.3.3) to express the FWHM bandwidth in terms of the peak transmission of the filter gives

$$\text{FWHM} = (1 + T_0)^{-1} \left[\sqrt{1 + 14T_0^2 + T_0^4} - (1 - T_0)^2 \right]^{1/2} W \quad (5.3.4)$$

where T_0 is the peak transmission of the filter given by (5.2.6). The expression obtained above confirms the fact that as the bandwidth of the proposed filter decreases, the peak transmission also decreases or alternatively, the insertion loss of the filter increases. For very small values of T_0 the bandwidth of the filter can be approximated by

$$\text{FWHM} \approx \sqrt{2T_0} W \quad (5.3.5)$$

Hence, to achieve a decrease in the bandwidth of a single cavity filter by a factor of 2, the coupler tap ratio required is 0.79 (from (5.3.3)) and the peak transmission (from (5.3.4)) is 0.116 giving an insertion loss of 9.3 dB.

5.4 *Tuning Range Of The Filter*

In order to attain a high peak transmission, a low value of α must be chosen. However, as is evident from Fig. 15, this results in the loss of the desirable property of increase in the tuning range (FSR) obtainable by using two F-P cavities in tandem. In other words, as may be noted from Fig.15, with a low value of α ($\alpha=0.1$) and with the two cavities having slightly different tuning ranges ($\text{FSR}_2 = (5/4).\text{FSR}_1$), the tuning range of the feedback filter is almost equal to that of a single F-P filter while the tandem filter achieves a fivefold increase in tuning range relative to a single F-P (from (3.2.1)). Hence, to achieve an

improvement in tuning range given by (3.2.1) by employing the vernier effect, the tap ratio must be moderately high. The decrease in peak transmission seen in Fig. 16 can be compensated for by using an amplifier as discussed in a later section.

5.5 Secondary Peak Behavior

As was noted earlier, the transmission spectrum of the filter with unequal FSR's has, in addition to main peak resonances, a number of smaller secondary resonances. These correspond to those frequencies for which only one cavity is in resonance. Considering the first secondary resonance which occurs at a frequency offset of FSR_1 (assuming that $FSR_2 > FSR_1$) from the main resonance we note that,

$$G(FSR_1) = 1 \quad (5.5.1)$$

and

$$H(FSR_1) = \frac{1}{1 + \frac{4R_2}{(1-R_2)^2} \sin^2 \left[\frac{\pi(FSR_2 - FSR_1)}{FSR_2} \right]}$$

$$\approx \left(\frac{W}{2\Delta FSR} \right)^2 \quad (5.5.2)$$

Hence,

$$T(FSR_1) \approx \frac{(1 - \alpha)^2}{1 - \alpha^2 \cdot 1 \cdot \left(\frac{W}{2\Delta FSR} \right)^2} \approx (1 - \alpha)^2 \quad (5.5.3)$$

Hence, in order to reduce the magnitudes of the secondary peaks and consequently the crosstalk, α must be as high as possible. In other words, it is advisable to have a high tap ratio.

The secondary resonances occur in pairs. The second member of this pair occurs at a frequency offset of FSR_2 from the main resonance. Here, we note that (in an analogous manner)

$$H(\text{FSR}_2) = 1 \quad (5.5.4)$$

and

$$G(\text{FSR}_2) \approx \left(\frac{W}{2\Delta\text{FSR}} \right)^2 \quad (5.5.5)$$

Hence,

$$T(\text{FSR}_2) \approx \frac{\left(\frac{W}{2\Delta\text{FSR}} \right)^2 \cdot (1 - \alpha)^2}{1 - \alpha^2 \cdot \left(\frac{W}{2\Delta\text{FSR}} \right)^2 \cdot 1}$$

$$\therefore T(\text{FSR}_2) \approx \left(\frac{W}{2\Delta\text{FSR}} \right)^2 \cdot (1 - \alpha)^2 \ll 1 \quad (5.5.6)$$

Since ΔFSR is large compared to W (typical values are $W = 200$ MHz and $\Delta\text{FSR} = 1$ GHz) this term is negligible compared to the first term given by (5.5.3). Thus, this member of the secondary resonance pair does not play a significant role in increasing crosstalk and may be ignored.

5.6 *Impact Of Delay In The Feedback Path*

As was pointed in section 3.5, when a filter is built using multiple separate cavities, care must be taken to suppress the distortion caused by intercavity resonances by separating the cavities by a distance greater than the coherence length of the source. Hence

$$L \gg L_C \quad (5.6.1)$$

where L is the length of fiber between the two cavities and L_C is the coherence length of the source. The coherence length is related to the laser linewidth $\Delta\nu$ by [5]

$$L_C = \frac{c}{2\pi n \Delta\nu} = \frac{c\tau_c}{n} \quad (5.6.2)$$

where c is the velocity of light in vacuum, n is the index of refraction of the medium and τ_c is the laser

coherence time. From (5.6.1), we can conclude that the delay τ suffered by a signal in the feedback path is related to the laser's coherence time τ_c by

$$\tau \gg \tau_c \quad (5.6.3)$$

To minimize intersymbol interference, the delay in the feedback path must be much smaller than the bit period. In other words

$$\tau \ll \frac{1}{R} \quad (5.6.4)$$

where R is the signal bit rate. From (5.6.3) and (5.6.4), we can conclude that

$$R \ll \Delta\nu \quad (5.6.5)$$

This implies that this filter would be well suited only for highly incoherent systems. In the frequency domain, the effect of the delay is to introduce an oscillatory term into the frequency response given by (5.2.5). If (5.6.4) is satisfied, the period of this oscillation is large compared to the frequencies of interest and this oscillation may be neglected.

5.7 Amplifier In The Forward Path

As was evident from the earlier sections, the proposed filter suffers from the problem of having contradictory requirements for the value of α to achieve a high peak transmission and a narrow bandwidth simultaneously. To address this problem, a possible solution involves incorporating a wideband amplifier (with respect to the filter's FSR) in the filter's forward path. Placing the amplifier in the feedback path would be undesirable as it would reduce the peak transmission further instead of improving it. The response of the filter with an amplifier in its forward path is analyzed in this section.

The power transmission spectrum of the filter is now given by

$$T(f) = \frac{(1-\alpha)^2 AG(f)}{1-\alpha^2 AG(f)H(f)} \quad (5.7.1)$$

where A is the wideband gain of the amplifier. Hence, using (5.3.1) we get

$$T(w) = \frac{(1 - \alpha)^2 A (1 + w^2)}{(1 + w^2)^2 - \alpha^2 A} \quad (5.7.2)$$

where $w = 2f/W$. The peak transmission of the filter is now given by

$$T(0) = \frac{(1 - \alpha)^2 A}{1 - \alpha^2 A} \quad (5.7.3)$$

while its FWHM bandwidth is obtained by setting $T(\epsilon) = T(0)/2$ to give

$$\text{FWHM} = \epsilon W = \left[\sqrt{\alpha^4 A^2 - \alpha^2 A + 1 - \alpha^2 A} \right]^{1/2} \cdot W \quad (5.7.4)$$

The dependence of the peak transmission and the FWHM bandwidth of the filter on the gain of the amplifier in the forward path given by (5.7.3) and (5.7.4) respectively for a filter with $\alpha = 1/2$ has been plotted in Fig. 17. As is evident both from the expressions as well as the figure, the filter bandwidth decreases while the peak transmission increases with increasing amplifier gain. For example, a gain of 3 dB ($A=2$) results in both no insertion loss ($T(0)=1$) and a narrowing of the filter bandwidth to 0.605 that of a single cavity filter.

5.8 Conclusion

Based on the preceding discussion regarding the choice of the coupler tap ratios required in order to increase the peak transmission of the filter as well as to decrease the magnitude of the secondary peaks and the FWHM bandwidth of the filter, we observe that both these requirements cannot be met simultaneously by using a directional coupler as a power summer on the left side of the filter. However, by compensating for the lower peak transmission by using a more sensitive receiver (eg. APD's) or by incorporating an amplifier in the forward path of the filter, it is advisable to choose a high value for α so as to reduce crosstalk as well as to increase the tuning range of the filter. We may, thus, conclude that the proposed structure provides improvement in bandwidth and tuning range over that of a single cavity filter by a suitable choice of the tap ratio of the couplers. Additionally, without replacing the two cavities used in the

filter, the filter characteristics can be changed by changing the tap ratio of the couplers. This filter can be used in incoherent communication systems employing optical amplifiers to suppress the wideband spontaneous-spontaneous beat noise introduced by these amplifiers. Also, the use of a passive filter in a feedback configuration around an optical amplifier may provide a means for varying the effective response of the amplifier without changes to the active structure.

6.0 FDMA M-ary FSK Star Networks

Analogous to the radio frequency Frequency Division Multiple Access (FDMA) systems currently being employed in the telecommunications arena, optical frequency FDMA systems are now making their appearance. The underlying principle of the FDMA network is that a unique optical carrier frequency from among a comb of the same is assigned to each active user either permanently or dynamically for the duration of a session. While amplitude-shift-keying (ASK) modulation techniques are attractive from the point of view of their narrower spectral spread, thus enabling more channels to be packed into the available spectrum, the chirping produced as a result of direct modulation of the laser or alternatively, the additional insertion loss produced by the external modulator are major demerits of this scheme. Likewise, phase-shift-keying (PSK) is not employed owing to the need for external modulators and extremely stable narrow linewidth lasers both as sources as well as local oscillators in a coherent detection scheme. Instead, frequency-shift-keying (FSK) is an attractive alternative since it allows direct frequency modulation without the need for lossy external modulators. In fact, the undesirable feature of chirping found in ASK modulation schemes is put to good use here to generate FM. While coherent FSK schemes offer improved receiver sensitivity, the need for tunable local oscillators and polarization controllers is avoided in incoherent detection schemes employing fiber Fabry-Perot (FFP) filters at the expense of reduced receiver sensitivity [14]. In the previous chapters we discussed the operation and the principal performance parameters of F-P filters (single and multicavity structures). In this chapter, an application of the F-P filter in a star network is discussed.

Based on an earlier study [14] of binary FSK FDMA networks, it was evident that an FDMA star network employing M-ary FSK ($M > 2$) modulation was a feasible alternative. Among the attractive features of this modulation scheme are its reduced electrical bandwidth needs with no additional power requirements. Also, in a thermal noise limited situation, M-ary FSK affords lower error rates than binary PSK (BPSK) at identical power levels. However, these bonuses are gained at the expense of increased optical bandwidth and hardware complexity.

The following sections will discuss the proposed network architecture, source laser performance requirements, crosstalk power penalty in an M-ary FSK system and finally error performance and dispersion power penalty in a BFSK system.

6.1 Network Architecture

As seen in Fig. 18, the FDMA network we are proposing has a primary single-mode passive $N \times N$ star coupler and N secondary $1 \times M$ passive splitters. Each of the N terminals connected to the inputs of the primary star is assigned a unique transmission wavelength. Thus, the primary star serves the dual purpose of multiplexing and broadcasting. Each of the N secondary $1 \times M$ splitters broadcasts the multiplexed outputs from the star to M FFP filters to enable the demodulation and detection of the M-ary FSK signal. Thus, the network employs a total of $M \cdot N$ FFP filters. The filters have identical parameters (bandwidth, finesse and tuning range) and are tunable over the entire transmission spectrum of the network. Alternatively, the filtering can be done in two steps with a tunable wideband filter (with a large FSR) to select the appropriate band followed by a narrowband filter (with a smaller FSR) to select the desired channel from the band. This approach is particularly feasible for networks in which the number of users increases significantly in comparison to the number of users the network was originally designed for. Additionally, the primary wideband filter need not be continuously tunable over the entire transmission spectrum of the network while the secondary narrowband filters need not have a tuning range as large as the entire transmission spectrum of the network. Each FFP is centered at one of the M frequencies and is connected to an independent photodetector. Thus, the M-ary FSK signal is converted to an M-ary ASK signal. The decision as to which of the M frequencies was transmitted is made by the receiver by

comparing the relative amplitudes of the M filter outputs. The symbol with the highest amplitude is selected as the most probable transmitted symbol. To minimize error rate degradation due to dispersion, the entire network is built using single-mode fibers. As is evident, the two-level splitting introduces a considerable insertion loss which will have to be compensated for by using high transmission powers or optical amplifiers.

6.2 Source Laser Characteristics

As pointed out in the introductory paragraph, the ability to perform direct FM modulation of the laser is one of the factors which makes FSK modulation attractive. However, in order to minimize waveform distortion and the resulting error rate, the FM response of the lasers must be flat over a wide range of modulation rates. In other words, the FM efficiency (frequency deviation per unit current) must be constant over a wide range of modulation rates. However, owing to the coexistence of the fast responding carrier density modulation effect and the slow responding temperature change effect in the active layer, the FM response of the laser may be V-shaped. Owing to the heating effects in the laser which are produced by the low frequency components of the data stream, the laser drive circuitry must be equalized to rectify this problem. Additionally, a large FM efficiency is desirable so as to achieve frequency modulation with minimal intensity modulation. Also, narrow linewidth sources are essential to minimize the error rate. A strong candidate for such a source is a 1.5 μm phase-tunable DFB (PT DFB) laser with high FM efficiency (10 GHz/ma) and a flat FM response up to 500 MHz [15].

6.3 Network Crosstalk Power Penalty

In this section, the dependence of crosstalk interference on the frequency separation between the signal components of an M-ary FSK signal and the corresponding channel spacing in the frequency domain is analyzed.

The M signals in the signal set can be represented as (refer Fig. 19a)

$$s_i(t) = A \cos(\omega_0 t + \theta_0 + (i-1)\omega_d t) \quad , i = 1, 2, \dots, M \quad (6.3.1)$$

where ω_0 is the carrier frequency and ω_d is the frequency deviation between adjacent signal frequencies in rads/s (f_d is the corresponding frequency deviation in Hz). Additionally, ω_c is the frequency separation between adjacent channels in rads/s (f_c is the corresponding frequency separation in Hz). Also, B is the channel symbol rate, W is the FWHM bandwidth of a single FFP cavity and P is the total power in the channel.

The maximum crosstalk interference in a channel occurs in the filters centered at the lowest and highest signal frequencies where signal leakage can occur both from the same as well as adjacent channels. Hence, the average crosstalk power penalty was computed for this worst-case scenario. The power penalties for a single FFP filter, a tandem (two cavity) filter with an isolator between the two cavities and a feedback filter were computed.

In order to compute the crosstalk interference, the power spectrum of a continuous phase M-ary FSK signal must be investigated. The power spectrum of a continuous phase M-ary FSK signal with large deviation index μ ($\mu = f_d/B > 1$) consists of M peaks spaced f_d apart of approximate width $B/2$ decaying as f^{-4} far from the peaks [16] as shown in Fig. 19b. Hence, as a crude approximation for an M-ary FSK signal with a large modulation index, the crosstalk can be represented as the sum of two components namely [14]

- (a) transmission through the filter of the unmodulated adjacent signal frequency carriers and
- (b) tails of the modulated adjacent signal frequency spectra integrated over the filter passband.

Crosstalk contributions from other channels in the network have been ignored. Each component is obtained below as shown. The transmission spectra of a single cavity filter and a tandem filter are given by (3.5.1) and (3.5.2) respectively while that of a feedback filter is given by (from (5.3.2))

$$T(f) \approx \frac{(1-\alpha)^2 \left[1 + \left(\frac{2f}{W} \right)^2 \right]}{\left[1 + \left(\frac{2f}{W} \right)^2 \right]^2 - \alpha^2} \quad , |f| < W \ll \text{FSR}_1, \text{FSR}_2 \quad (6.3.2)$$

$$\approx \frac{(1-\alpha)^2 \left(\frac{2f}{W}\right)^2}{\left(\frac{2f}{W}\right)^4 - \alpha^2}, \quad W \ll \Delta f \ll \text{FSR}_1, \text{FSR}_2$$

Since we are computing the average worst-case (i.e., the average crosstalk interference power in the worst-case signal frequencies) crosstalk interference, the power in each peak of the power spectrum is $1/M$ of the total power in the channel (since the probability of occurrence of each of the M signals in the signal set is equal). In other words, the power in each signal component is P/M . Hence, assuming that $f_c = Mf_d$, the (a) crosstalk component is given by

$$P_{I(a)} = \frac{P}{M} \cdot [T(f_d) + T(f_c - (M-1)f_d)]$$

$$\therefore P_{I(a)} = \frac{2P}{M} \cdot T(f_d) \quad (6.3.3)$$

where $f_d > W$.

To minimize crosstalk penalty, the filter bandwidth should be small. However, if the bandwidth is too small, there will be a loss of signal power. Hence, the minimum system bandwidth is assumed to be equal to the symbol rate. The (a) crosstalk component for each of the three filters is given (single, tandem and feedback respectively) by

$$\text{Single Filter} \quad P_{I(a)} = \frac{2P}{M} \cdot (2\mu)^{-2} \quad (6.3.4)$$

$$\text{Tandem Filter} \quad P_{I(a)} = \frac{2P}{M} \cdot (2\mu)^{-4} \quad (6.3.5)$$

$$P_{I(a)} = \frac{2P}{M} \cdot (1 - \alpha)^2 \frac{(2\mu)^2}{(2\mu)^4 - \alpha^2}$$

$$\text{Feedback Filter} \quad P_{I(a)} \approx \frac{2P}{M} \cdot \frac{(1 - \alpha)^2}{(2\mu)^2} \quad (6.3.6)$$

where $\mu = f_d/B$.

To obtain the (b) crosstalk component, we may proceed as follows. Since, the power spectrum of a continuous phase M-ary FSK signal with large deviation index has peaks decaying as f^{-4} far from the peaks, the power spectrum can be approximated by a squared Lorentzian function given by

$$S(\delta f) = \frac{A}{\left[1 + K\left(\frac{\delta f}{B}\right)^2\right]^2}$$

where δf is the frequency deviation from the peak and K and A can be determined by using the knowledge of the linewidth ($B/2$) of each peak and the power in each peak (P/M) respectively. Thus, the power spectrum of the M-ary FSK signal can be approximated by

$$S(\delta f) = \frac{8(\sqrt{2} - 1)^{1/2}P}{M\pi B \left[1 + (\sqrt{2} - 1)\left(\frac{4\delta f}{B}\right)^2\right]^2} \quad (6.3.7)$$

The (b) crosstalk component can be approximated by the product of the magnitude of the adjacent signal frequency spectrum at the center of the passband and the total area (N) under the filter passband. Thus, it is given by

$$P_I(b) = N[S(f_d) + S(f_c - (M-1)f_d)]$$

$$\therefore P_I(b) = 2N.S(f_d) \quad (6.3.8)$$

assuming that $f_c = Mf_d$. In (6.3.8) above, N is obtained by integrating the transmission spectrum of each filter over all f (using the expression corresponding to $|f| < W$). Thus, for the single, tandem and feedback filter respectively, we get

$$N = \frac{\pi W}{2} \quad (6.3.9)$$

$$N = \frac{\pi W}{4} \quad (6.3.10)$$

$$N = \frac{\pi W}{4} \cdot (1 - \alpha)^2 \left(\frac{\sqrt{1+\alpha} + \sqrt{1-\alpha}}{\sqrt{1-\alpha^2}} \right) \quad (6.3.11)$$

The relationship between the filter bandwidth and the FWHM bandwidth of a single cavity W is obtained from (3.5.4) and (5.3.3) for a tandem (two cavities with an isolator) and a feedback filter respectively. Using these results and the expressions for N obtained above, the (b) crosstalk component for the single, tandem and feedback filter respectively is given by

$$P_{I(b)} \approx \frac{8(\sqrt{2} - 1)^{-3/2} P}{M} \cdot (4\mu)^{-4} \quad (6.3.12)$$

$$P_{I(b)} \approx \frac{4(\sqrt{2} - 1)^{-2} P}{M} \cdot (4\mu)^{-4} \quad (6.3.13)$$

$$P_{I(b)} = \frac{4(\sqrt{1+\alpha} + \sqrt{1-\alpha})(1-\alpha)^2(\sqrt{2}-1)^{-3/2}P}{M \cdot \sqrt{1-\alpha^2} \cdot [\sqrt{1-\alpha^2+\alpha^4} - \alpha^2]^{1/2}} \cdot (4\mu)^{-4} \quad (6.3.14)$$

The total crosstalk interference (P_I) in each of the three cases is obtained by summing the corresponding (a) and (b) components. By comparing equations (6.3.4) and (6.3.12), (6.3.5) and (6.3.13) and finally (6.3.6) and (6.3.14) in pairs which correspond to the (a) and (b) crosstalk components respectively for each of the three cases, we note that the (a) component is dominant in a single cavity filter due to the weak cutoff in the passband while the components are comparable in size in the tandem and the feedback filter due to a stronger cutoff in the passband. The crosstalk interference can be quantified in terms of a power penalty which refers to the increase in signal power required to achieve the desired bit error rate (BER). The crosstalk power penalty (p_I) is defined in terms of the decrease in the off-on power increment giving rise to the expression [14]

$$p_I = -10 \cdot \log \left(1 - \frac{P_I}{P} \right) \quad (6.3.15)$$

It follows from summing equations (6.3.4) and (6.3.12), (6.3.5) and (6.3.13) and lastly (6.3.6) and (6.3.14) that for a power penalty of 0.1 dB, the modulation index for a quaternary ($M=4$) FSK signal is 2.4 for a single cavity filter, 1.25 for a tandem filter and 1.3 for a feedback filter with tap ratio α being 1/2 as

compared with 3.2, 1.5 and 1.75 respectively for a BFSK ($M=2$) signal. Thus, for a given filter FSR, a greater number of channels can be accommodated in a tandem or a feedback filter in comparison to a single cavity FP filter. The expressions for crosstalk derived here assume that the power in the channel is equally divided among all the signal frequencies (i.e., all M signal components occur with equal probability). In the preceding discussion, the M frequencies comprising a single channel were chosen far enough apart in the frequency domain so as to form a set of orthogonal signals. The set of M signals in the M -ary signal space can be visualized as points in the M -dimensional space with one point on each of the coordinate axes. As is easily seen, the minimum Euclidian distance cannot be increased even by expanding the signal set without increasing the signal power. Thus, for example, Trellis Coded Modulation (TCM) coding, which uses redundant nonbinary modulation through signal set expansion along with a finite-state encoder to generate coded signal sequences, will not produce any coding gain in the case of orthogonal signal sets [17]. However, if the signal set is not orthogonal owing to the desire to achieve more signal frequencies or channels, imperfect filters or due to other reasons, coding might offer an advantage. Thus, under identical crosstalk penalty requirements, the frequency spacing between signal components may be less for M -ary FSK than for BFSK if suitable coding techniques are employed. Additionally, the receiver sensitivity of the former is better than that of the latter by approximately a factor of $\log_2 M$ since the required energy per pulse is about the same in both cases [18]. Lastly, the throughput for a given filter FSR and signaling rate drops for $M > 4$ in comparison to that for BFSK modulation. Although both power and bandwidth efficiency for $M=4$ can be better than that for $M=2$, this needs to be balanced against the added complexity of an $M=4$ receiver.

The remaining sections of this chapter deal with error performance and dispersion penalty in a incoherent binary FSK modulation scheme.

6.4 Error Performance

This section analyzes the error performance of an incoherent BFSK transmission system. The link employs an optical amplifier as a preamplifier. As pointed out in Section 6.1, optical filters are used to convert the FSK signal into an ASK signal prior to detection. The error performance of the system

employing two different configurations, one with the receiver having one F-P filter and the other having two F-P filters are analyzed and compared. The motivation for performing this analysis is to determine if there is any improvement in performance to be gained by using two filters instead of one. It is assumed that the received signal is corrupted by the presence of amplified spontaneous emission noise introduced by the optical amplifier and electrical thermal noise generated in the receiver.

Assuming that the received optical signal is given by

$$z(t) = a \cdot \cos(\omega_i t + \theta) + p(t) \quad , i = 0, 1 \quad (6.4.1)$$

where $p(t)$ represents the amplified spontaneous emission noise introduced by the optical amplifier, the filter outputs in the two cases (one and two filter receivers) are as expressed below. The filter outputs refer to the detected electrical signal.

In the one filter receiver with the filter centered at the 1 frequency, the filter output when a 1 or a 0 is transmitted is given respectively by

$$z_1 = \frac{1}{2} \cdot (a+x_1)^2 + \frac{y_1^2}{2} + n \quad (6.4.2)$$

$$z_0 = \frac{1}{2} \cdot (x_0^2 + y_0^2) + n \quad (6.4.3)$$

where n is the additive electrical thermal noise introduced by the receiver circuitry. It may be noted that n is a zero mean Gaussian random variable with variance σ_t^2 (thermal noise power). It is implicitly assumed in the above that all of the filtering is done optically. In practice, the optical filter bandwidth is much larger than the bit rate in which case post-detection filtering may also be done. However, this has not been considered here since we are concerned only with the relative sensitivity of the two receiver structures.

In the two filter receiver, the two filter outputs when a 1 is transmitted are

$$z_1 = \frac{1}{2} \cdot (a+x_1)^2 + \frac{y_1^2}{2} + n_1 \quad (6.4.4)$$

$$z_0 = \frac{1}{2} \cdot (x_0^2 + y_0^2) + n_0 \quad (6.4.5)$$

where z_1 and z_0 are the outputs of the filters centered at the 1 and 0 frequencies respectively and n_1 and n_0 are the corresponding thermal noise terms. Similarly, when a 0 is transmitted, the filter outputs are

identical but in reverse order. In the four expressions given above, x and y are the inphase and quadrature components of the amplified spontaneous emission noise. The $\{x_i\}$ and $\{y_i\}$ are independent and identically distributed (i.i.d) zero mean Gaussian random variables with variance σ^2 (noise power) and the x_i 's and y_i 's are orthogonal to each other for the same i . Also, n_1 and n_0 are i.i.d zero mean Gaussian random variables with variance σ_t^2 .

The mean and variance of the filter output in the one filter receiver are

$$\mu_1 = \frac{a^2}{2} + \sigma^2 \quad \sigma_1^2 = a^2\sigma^2 + \sigma^4 + \sigma_t^2$$

$$\mu_0 = \sigma^2 \quad \sigma_0^2 = \sigma^4 + \sigma_t^2$$

when a 1 and 0 are transmitted respectively. The probability of error, assuming that the threshold voltage is chosen to make the errors of both kinds (i.e. mistaking a 1 for a 0 and vice-versa) equal, for a single filter receiver is given by (assuming that z_1 is Gaussian)

$$P_e = Q\left(\frac{\mu_1 - \mu_0}{\sigma_1 + \sigma_0}\right) \quad (6.4.6)$$

where

$$Q(y) = \frac{1}{\sqrt{2\pi}} \cdot \int_y^\infty \exp\left(-\frac{x^2}{2}\right) dx$$

The Gaussian approximation should be better the larger the thermal noise component. It is surprisingly good [19] even when thermal noise is absent (in fact, the Gaussian approximation gives a result for the receiver sensitivity only slightly off that obtained from using the exact distribution). Hence, the error probability is

$$P_e = Q\left(\frac{a^2/2}{\sqrt{a^2\sigma^2 + \sigma^4 + \sigma_t^2} + \sqrt{\sigma^4 + \sigma_t^2}}\right) \quad (6.4.7)$$

However, in the signal spontaneous beat noise limit,

$$\frac{\sigma_i^2}{\sigma^4} \rightarrow 0 \quad \text{and} \quad \frac{a^2}{\sigma^2} > 1 \quad (6.4.8)$$

$$\Rightarrow P_e \approx Q\left(\frac{a}{2\sigma}\right) \quad (6.4.9)$$

For, the two filter receiver, let

$$z = z_1 - z_0 = \frac{1}{2} \cdot (a^2 + 2ax_1 + x_1^2 + y_1^2 - x_0^2 - y_0^2) + n_1 - n_0 \quad (6.4.10)$$

The mean and variance of z (both when a 1 or a 0 occur) are

$$\langle z \rangle = \frac{a^2}{2} \quad \sigma_z^2 = a^2\sigma^2 + 2\sigma^4 + 2\sigma_i^2$$

Hence, the error probability for the two filter receiver is given by (assuming z is Gaussian)

$$P_e = \text{Prob}\{z < 0\} = Q\left(\frac{a^2}{2\sqrt{a^2\sigma^2 + 2\sigma^4 + 2\sigma_i^2}}\right) \quad (6.4.11)$$

Again, in the signal spontaneous beat noise limit, using (6.4.8) we get

$$P_e \approx Q\left(\frac{a}{2\sigma}\right) \quad (6.4.12)$$

From (6.4.9) and (6.4.12) it may be noted that the SNR required for a given error performance is the same for both one and two filter receivers in the signal-spontaneous beat noise limit. However, to achieve a given performance, the single filter receiver requires an optimal setting of the threshold while the two filter receiver does not require adjusting a threshold. Additionally, the two filter receiver provides convenient automatic gain control (AGC).

6.5 Dispersion Penalty

This section discusses the impact of dispersion in terms of a power penalty in a binary FSK (BFSK) transmission system having a one-filter receiver. The analysis assumes a fiber having a Gaussian impulse response given by [20]

$$h(\tau) = \frac{1}{\sqrt{2\pi} \sigma_\tau} \exp\left(-\frac{\tau^2}{2\sigma_\tau^2}\right) \quad (6.5.1)$$

where σ_τ is the pulse width of the output pulse if an impulse is launched into the fiber and is given by

$$\sigma_\tau = D.L.\sigma_\lambda \quad (6.5.2)$$

where D is the dispersion coefficient of the fiber, L is its length and σ_λ is the spectral width of the source.

The Fourier transform of the fiber's impulse response is

$$H(\omega) = \exp\left(-\frac{\omega^2\sigma_\tau^2}{2}\right) \quad (6.5.3)$$

In the worst case, maximum dispersion penalty occurs for an alternating data sequence at bit rate R. For such a sequence, most of the power is carried by the frequency component at $\omega=\pi R$. Hence, the dispersion penalty in a single filter incoherent BFSK transmission system is

$$\alpha_{\text{ISI}} = -10.\log_{10} (H(\pi R)) \text{ dB}$$

Hence,

$$\alpha_{\text{ISI}} = 21.4 R^2 D^2 L^2 \sigma_\lambda^2 \text{ dB} \quad (6.5.4)$$

The expression obtained above implies that as the bit rate, transmission length or source spectral width increases the dispersion penalty also increases. Also, to minimize the dispersion penalty, operation in the low dispersion wavelength window is recommended. The impact of dispersion in the one and two-filter receiver configurations referred to in section 6.4 is also different. It can be noted that if the two filters are sampled simultaneously using a common clock, dispersion penalty is larger in the two filter receiver than in the single filter one since the group velocities of the two signal frequencies are different resulting in a delay between the two recovered clocks. However, if independently recovered clocks are used to sample the two filters, then the dispersion penalty is the same for both the cases.

6.6 *Conclusion*

In conclusion, this chapter discussed a proposed incoherent M-ary FSK star network employing F-P filters to convert the M-ary FSK signal to an M-ary ASK signal prior to detection. The attention to be paid to the FM modulation characteristics of the source and the necessary equalization of the laser drive circuitry was also discussed. The impact of crosstalk interference in terms of limitations on the frequency spacing between channels was also analyzed. The advantage of using M-ary FSK with associated coding techniques was brought out. Future work might involve the investigation of suitable coding techniques to achieve improved performance. In the concluding sections of this chapter, the merits and demerits of using a two-filter receiver instead of a one-filter one in an incoherent BFSK transmission system were discussed. The comparison was carried out with regards to the error performance and the impact of dispersion.

7.0 Multiwavelength Packet Switches and Networks

Ever since the introduction of optical fiber trunks in public telecommunication networks, the possibility of achieving throughputs of the order of 10^{12} bits/s. has become feasible. However, with the advent of multi-Gbits/s transmission systems, the lower speed electronic circuitry including electronic packet switches tend to become network bottlenecks. Thus, the need for high capacity packet switches for future broadband packet networks is increasingly evident. While single wavelength based photonic space division switching is a possible solution, it suffers from the need for high speed electronics in the switch. Alternatively, two major strengths of optical fiber technology, namely its inherent broadcast structure as well as the huge bandwidth of the fibers, can be exploited in multiwavelength photonic switches to achieve high capacity switching while employing moderate speed electronic circuitry. In Chapter 6, the architecture of a WDM based star network was discussed along with some of the associated system design issues.

The purpose of this chapter is to review and classify various proposals for multiwavelength packet switches that have appeared in the literature. They are classified into two categories namely the broadcast and select approach and the active wavelength routing approach. The former approach broadcasts incoming packets to all output ports followed by output buffering and lastly the processing of the packet headers to select the packets destined for a particular output. The power splitting inherent in this approach limits the number of ports the switch can have owing to the presence of a limited optical power budget. The latter

approach, on the other hand, employs input buffering and processing of the packet headers to determine the destination port followed by the active routing of the packets. The packet switches considered here consist, in general, of two internal networks, one for data transmission and the other for control of the switch itself. Additionally, the proposals considered here vary in their use of tunable or fixed wavelength transmitters and receivers. The concluding part of this chapter also examines the feasibility of implementing the proposals considered here as distributed networks.

7.1 The LAMBDANET Packet Switch

The LAMBDANET N -port switch consists of N input ports and N output ports [21]. Each input port has a unique wavelength associated with it while each output port has N fixed wavelength receivers to give a total of N^2 receivers. A passive wavelength insensitive star coupler performs the functions of multiplexing as well as broadcasting. Demultiplexing is achieved by means of a diffraction grating at each output port [22]. Since each output port has N receivers, information may be received by it from all the input ports simultaneously and asynchronously. Thus, LAMBDANET may be employed as a nonblocking, fully connected, data transparent (different data rates as well as formats can be supported simultaneously) packet switch. Besides unicasting, multicasting as well as broadcasting are supported by it too. The packets are output buffered and the header is processed to determine whether it is destined for a particular node. Output buffering avoids Head-Of-the-Line (HOL) effects but introduces output queueing delays due to processing and multiplexing overheads. In the absence of the HOL effect, extremely high throughputs are feasible and a bandwidth-distance product of $1.56 \text{ Tbits.s}^{-1}.\text{km}$ has been demonstrated [23]. Two major disadvantages of this proposal are the splitting loss associated with the star coupler which limits N and the multiplicity of receivers which scales as N^2 (a possible limitation for large N).

7.2 *The Photonic Knockout Switch*

Taking note of the fact that the probability of multiple packets from different input ports destined for the same output port decreases rapidly with increasing packet multiplicity under the assumption of uniform random incoming traffic, the number of receivers required at each output port may be drastically reduced. This is the central idea behind the working of the Knockout switch [21].

The Photonic Knockout switch associates a unique wavelength with each of the N input ports and has M ($M \ll N$) tunable receivers at each output port in contrast to the N fixed wavelength receivers in the former proposal. Depending on the number of packets (K) simultaneously arriving at various inputs destined for the same output port, all packets are transmitted ($K \leq M$) in the same time slot or a fair contest takes place ($K > M$) and the M winning packets are transmitted. The remaining are either dropped and have to be retransmitted or are buffered for one time slot [24] and compete in the next round with a higher priority allocated to them. The receivers are tuned to the appropriate wavelengths of the winning packets and the packets are received at the output. Interestingly, with the number of receivers limited to only 8 per output port, lost packet probabilities as low as 10^{-6} and smaller result under the assumption of uniform random traffic. Akin to the former proposal, this switch also uses output buffering to avoid HOL effects and displays an impressive delay and throughput performance. However, it needs tunable receivers resulting in the need for pretransmission coordination (so that the receiver may know which wavelength to tune to) and also the knockout algorithm adds additional complexity. Additionally, two level power splitting ($1 \rightarrow N$ and $1 \rightarrow M$) is carried out which further restricts the number of ports the switch can support from a power budget perspective. Among its advantages are that it provides for simple modular growth and maintenance procedures and is fault tolerant [25]. This switch is also nonblocking like the former.

7.3 *The FOX Switch*

The Fast Optical Cross-Connect (FOX) switch employs active wavelength routing to perform the switching function [21]. It incorporates two optical star networks internally, one dedicated for information

flow in each direction. In contrast to the previously discussed proposals, the FOX switch has fixed wavelength receivers and tunable transmitters at both the input and output ports. Incoming packets destined for a particular port are transmitted after tuning the transmitter to the appropriate wavelength. The FOX switch handles collisions (multiple packets arriving at an output port simultaneously) by retransmission. However, based on the same principle as the Knockout Switch, the delay and throughput performance of the FOX switch is impressive. Among its plus points are that it is nonblocking, fully connected and data transparent. In terms of its shortcomings, fast tuning stable laser transmitters are called for which may be expensive.

7.4 *The Shufflenet Packet Switch*

The ShuffleNet is a multistage switch based on a unidirectional bus architecture [21]. Akin to the LAMBDANET proposal, the ShuffleNet switch uses fixed wavelength transmitters and receivers. However, each input port employs two transmitters while each output port has two receivers. By virtue of this duality, ShuffleNet offers redundancy which can be exploited to achieve connectivity even in the event of congestion or node failure. The fixed wavelength interconnects are arranged in a perfect shuffle (hence the name) which has the capability of spreading traffic over the channels in a uniform manner if the offered load is uniformly distributed. The ShuffleNet combines the broadcast features of a star network and the multihop features of a ring network. Though the logical connectivity of the nodes conforms to a perfect shuffle pattern, the physical topology of the switch is compatible with star, tree and bus topologies [26]. Internal buffering is employed by the switch. For the bus topology, as the splitting losses are absent, extremely large switch fabrics are feasible. However, tapping losses may prove to be a limitation for the bus topology although wavelength selective taps may be used to partially overcome this. To ensure that the worst case insertion loss due to tapping, as seen by the farthest user, is not too large, a tree or a star topology may be employed. The ShuffleNet scores over the other proposals in terms of the absence of tunable transmitters and receivers and the lack of the need for pretransmission coordination [27]. The throughput per user decreases nearly as $1/\log_2 N$ as against $1/N$ for a single channel network. Thus, extremely high throughputs are feasible. However, larger delays may be encountered as the switch has

multiple stages.

7.5 *The HYPASS Switch*

The High Performance Packet Switching System (HYPASS) is a FOX-like switch with two internal star networks, one for data transmission and the other for control, with fixed wavelength receivers and transmitters in the output ports and tunable ones in the input ports [21]. This switch uses input buffering and the switching protocol is output controlled. Incoming packets are transmitted to the destination ports on the appropriate wavelengths only on receiving a request-to-send poll from the particular output port on its unique wavelength. The input port receiver is tuned to the appropriate wavelength of the control signal of the destination port in order to receive the poll. To eliminate the possibility of internal collisions, a variety of polling algorithms are employed depending on the traffic intensity and pattern. The tree polling algorithm is a particularly attractive option which offers a reduced average number of polling cycles even for heavy loads. The need for tunable transmitters and receivers at the input ports may prove to be unattractive.

7.6 *The Bellcore Star-Track Switch*

This switch also employs two internal networks, one an optical star network for data transmission while the other is an electronic ring network for control [21]. Fixed wavelength transmitters and tunable receivers are used at the input and output ports respectively. Switching is token driven. The token carries information about the destination ports, written into it by the input ports, to the output ports. This information is used by the output ports to tune the receivers to the appropriate wavelengths. Thus, multicasting can be easily achieved here. With fast tuning receivers and high-speed electronics, impressive peak throughputs in the range of 40-60 Gbits/s are feasible.

7.7 *Conclusion*

This chapter was aimed at providing an overview of a selection of multiwavelength packet switch proposals along with a discussion of their associated merits and demerits. All these proposals are, however, only in the research stage currently. As is evident, all the proposals considered here are viable candidates for implementing distributed networks. However, to overcome distance limitations due to loss in the fiber and other system components, broadband optical amplifiers (eg. TWA) may be employed. Also, transmission delay in the distributed network would have an impact on the buffer size at the ports depending on whether acknowledgements are used in the network protocol. Table 3 gives a summary of the salient features of each of the packet switches described in this chapter.

All these proposals use essentially passive networks with the intelligence in the terminals. An alternative is an active optical switch which in effect does a wavelength interchange. A method for doing this was recently proposed using fixed wavelength transmitters and receivers and tunable filters as the switching elements [28].

Table - 3
Multiwavelength Packet Switches

	I	II	III	IV	V	VI
Fixed λ xmitter	x	x		x	x(o/p)	x
Fixed λ receiver	x		x	x	x(o/p)	
Tunable xmitter			x		x(i/p)	
Tunable receiver		x			x(i/p)	x
# of recvs./port	N	M ($M \ll N$)	1	2	1	1
# of xmitters/port	1	1	1	2	1	1
# of internal n/ws	1(star)	1(star)	2(stars)	1(bus/tree/star)	2(stars)	2(star&ring)
# of stages	1	1	1	>1	1	1
Collision at o/p ports	NO	NO	YES	NO	NO	NO
Buffering	o/p	o/p	-	internal	i/p	-

I - LAMB DANET
 III - FOX Switch
 V - HYPASS

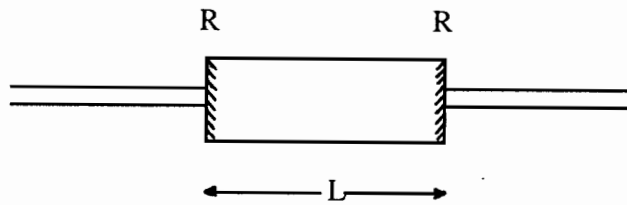
II - Knockout Switch
 IV - Shufflenet
 VI - STAR-Track

8.0 Conclusion

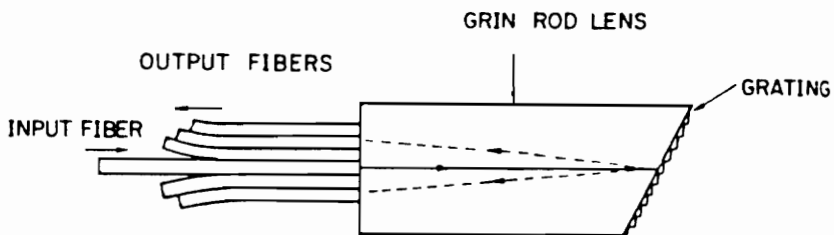
In conclusion, we outline the salient achievements of this thesis.

- The principle of operation of the F-P filter and its performance parameters have been defined and discussed.
- The improvement in performance achieved by using multimirror and multicavity F-P structures has been investigated in detail.
- A new technique for tuning F-P filters as well as a novel optical feedback based F-P filter has been proposed. Implementation of these techniques as well as further improvement in filter performance are potential areas for future research.
- The application of FFP filters in incoherent multiwavelength star networks and the associated concerns involving crosstalk and dispersion have been evaluated. Coding for M-ary FSK is another potential area for future research.
- Numerous multiwavelength network and switch proposals that have appeared in the literature along with their associated merits and demerits have been described. The design of new multiwavelength network architectures as well as interrelating technology, architecture and protocol

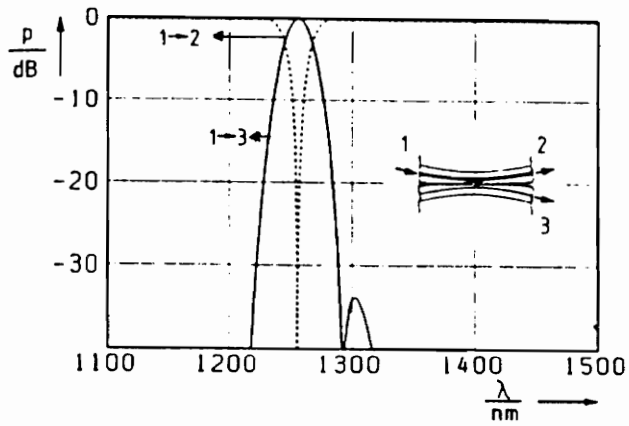
issues is another area appropriate for future research.



(a)



(b)



(c)

Figure 1a : A Fiber Fabry-Perot Filter

Figure 1b : A GRIN-rod Lens type Littrow Grating [4]

Figure 1c : Power transfer characteristics of an Asymmetrical Fiber Coupler [9]

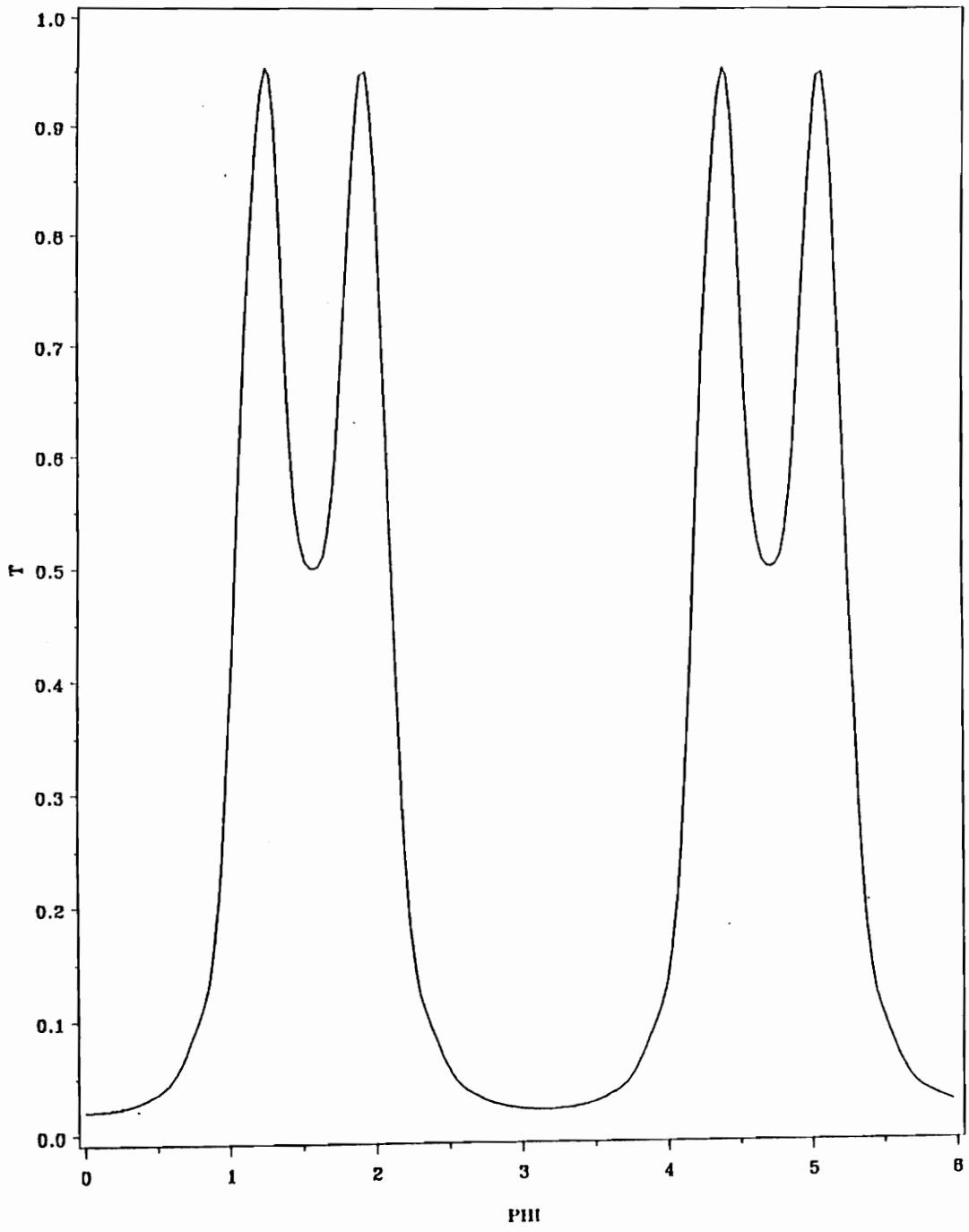


Figure 2 : Transmission Spectrum of a 3-Mirror F-P with equal reflectivities : $R_1 = R_2 = R_3 = 0.5$ and $FSR_1 = FSR_2$.

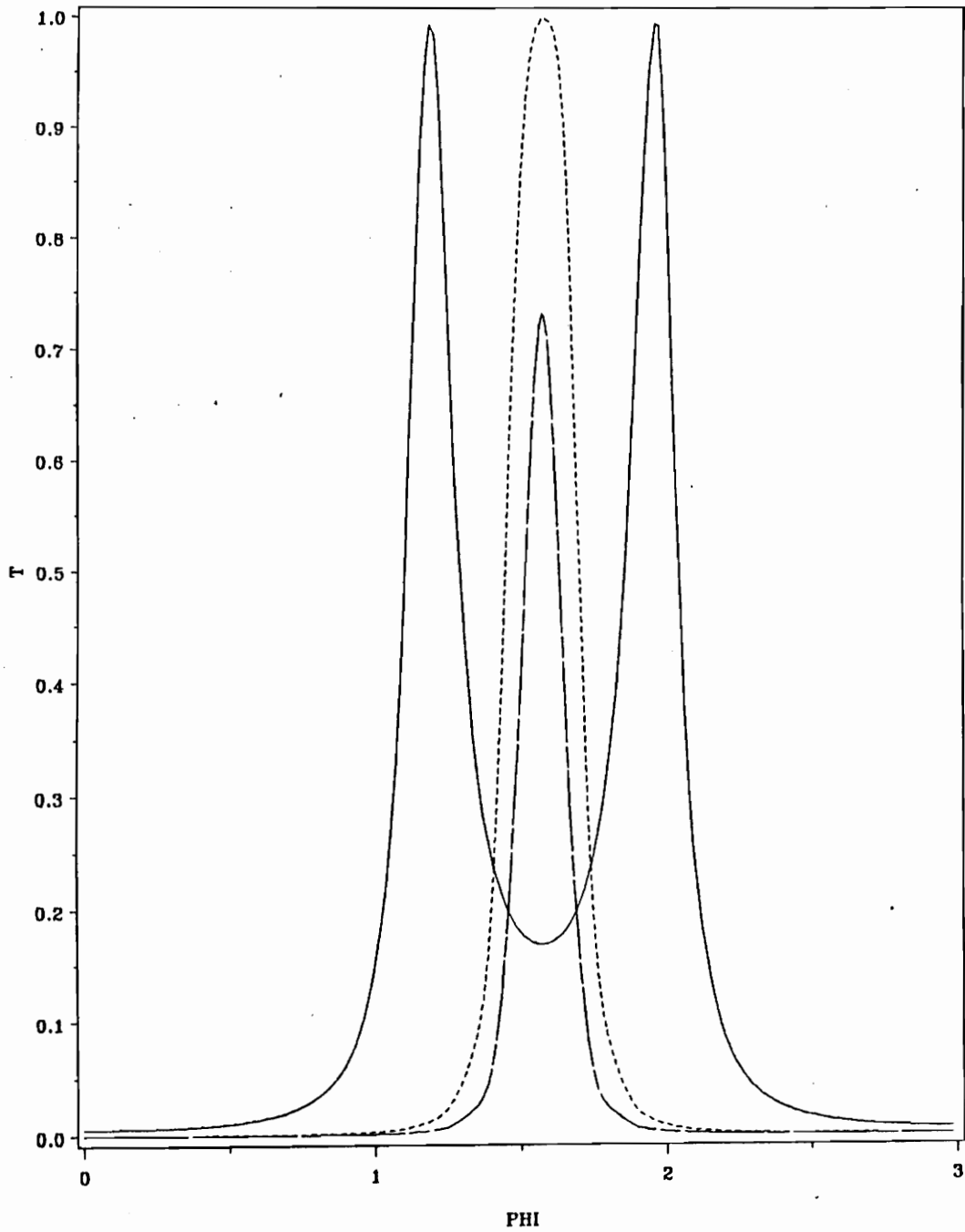


Figure 3 : Transmission Spectra of a 3-Mirror F-P : $R_1 = R_3 = 0.7$, $FSR_1 = FSR_2$ and different values of R_2 are chosen for each curve. The solid, dotted and dashed curves correspond to $R_2 = 0.5, 0.97$ and 0.99 respectively.

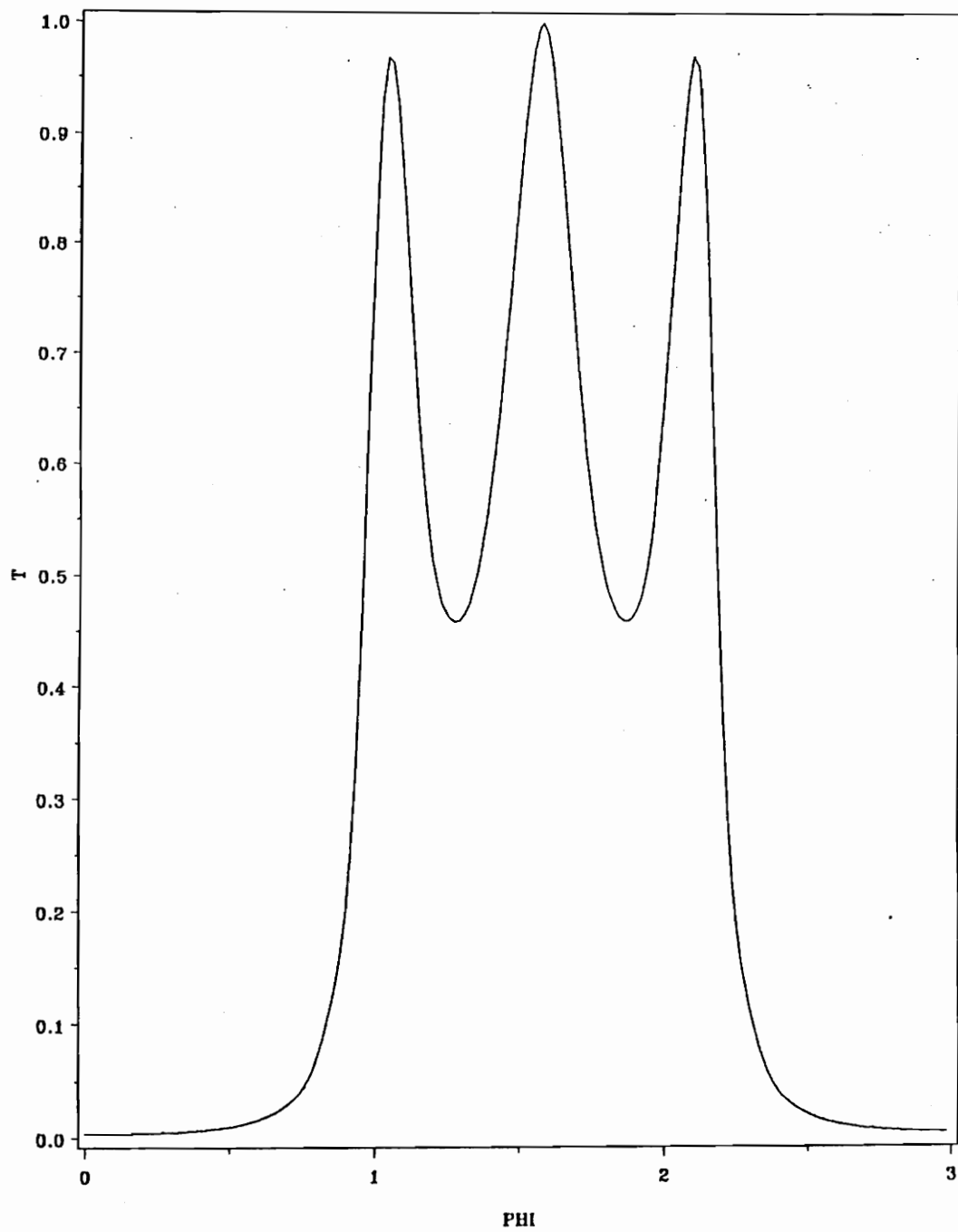


Figure 4 : Transmission Spectrum of a 4-Mirror F-P with equal reflectivities : $R_1 = R_2 = R_3 = R_4 = 0.5$ and $\text{FSR}_1 = \text{FSR}_2 = \text{FSR}_3$.

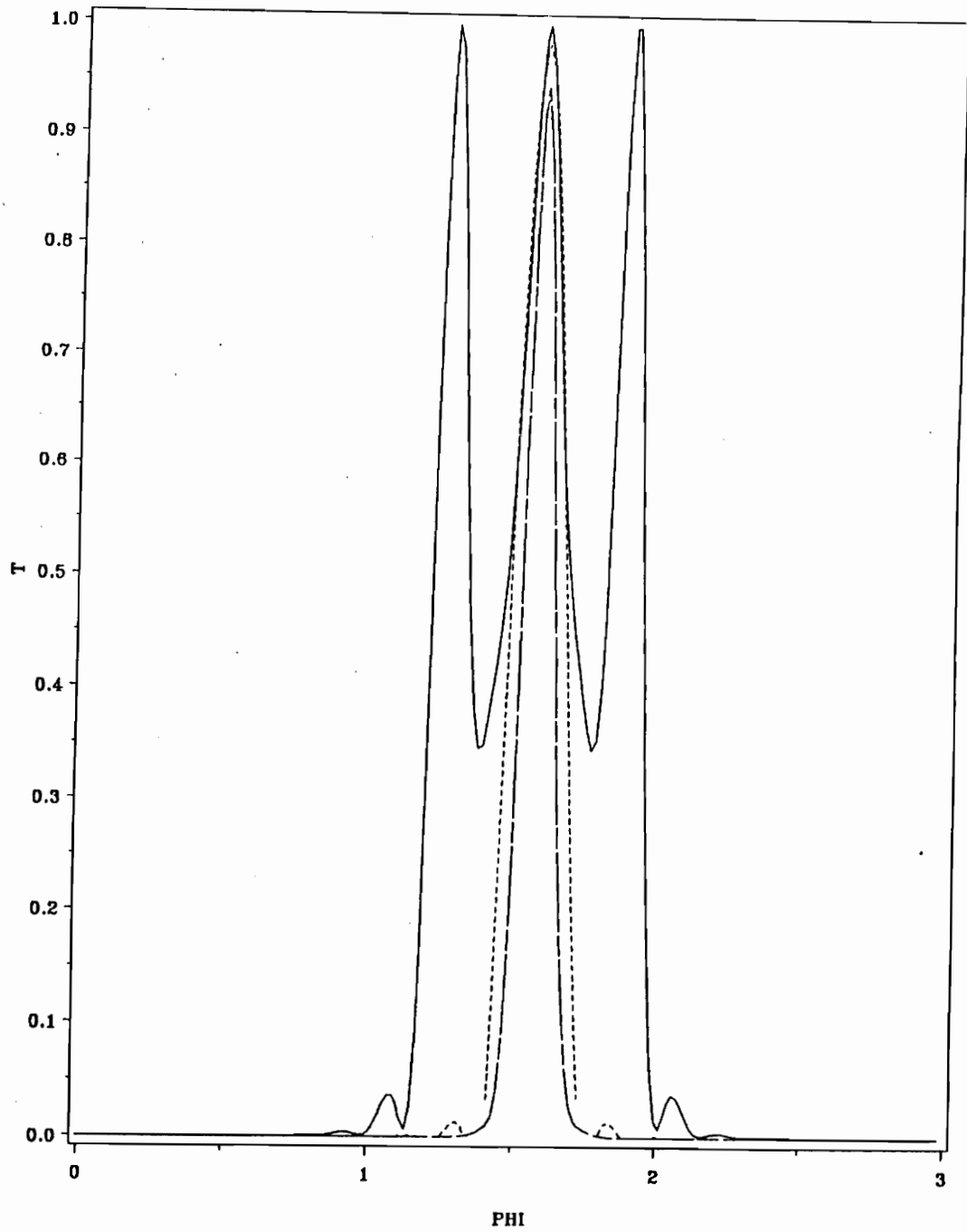


Figure 5 : Transmission Spectra of a 4-Mirror F-P : $R_1 = R_4 = 0.7$, $R_2 = R_3$ and $\text{FSR}_1 = \text{FSR}_3$. Different values of $R_2 = R_3$ are chosen for each curve. The solid, dotted and dashed curves correspond to $R_2 = R_3 = 0.8, 0.9842$ and 0.99 respectively.

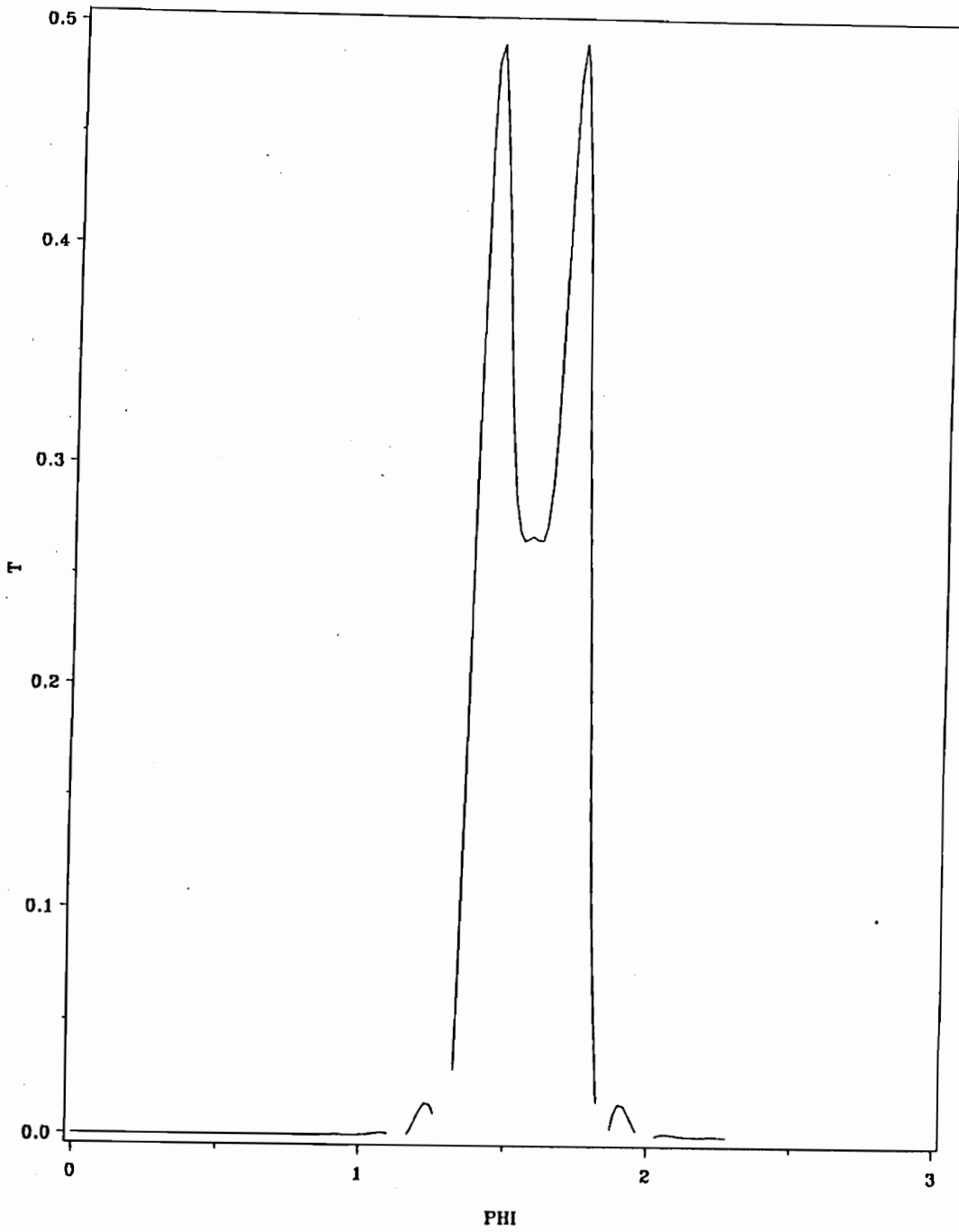


Figure 6 : Transmission Spectrum of a 4-Mirror F-P with unequal reflectivities : $R_1 = 0.7$, $R_2 = 0.9$, $R_3 = 0.9842$, $R_4 = 0.5$ and $FSR_1 = FSR_2 = FSR_3$.

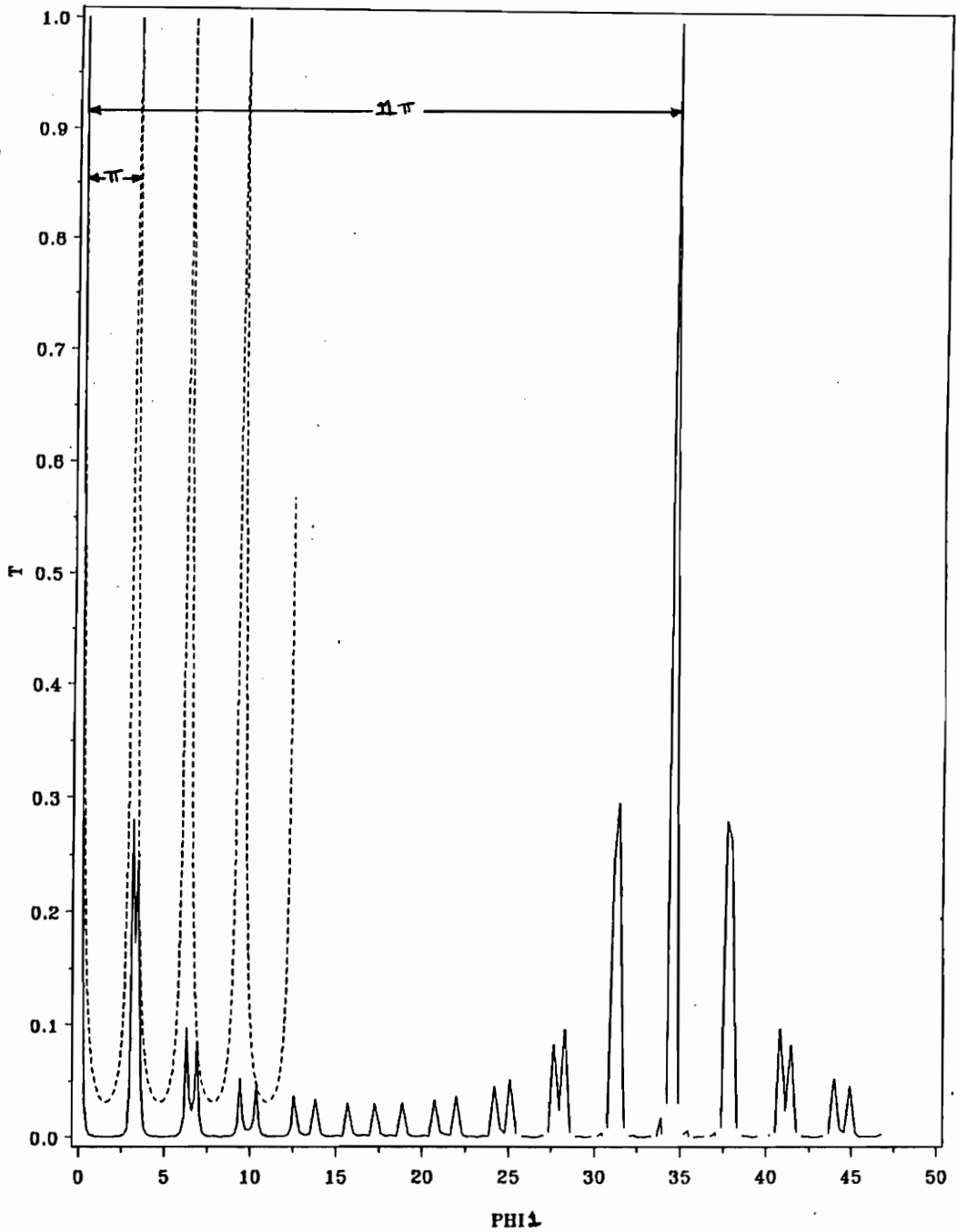


Figure 7 : Improvement in Tuning range in a 3-Mirror F-P : $R_1 = R_3 = 0.7$, $R_2 = R_{2,c} = 0.97$, $FSR_2 = (11/10) \cdot FSR_1$. The improvement is elevenfold. The solid and dashed curves correspond to the 3 and 2 mirror filters respectively.

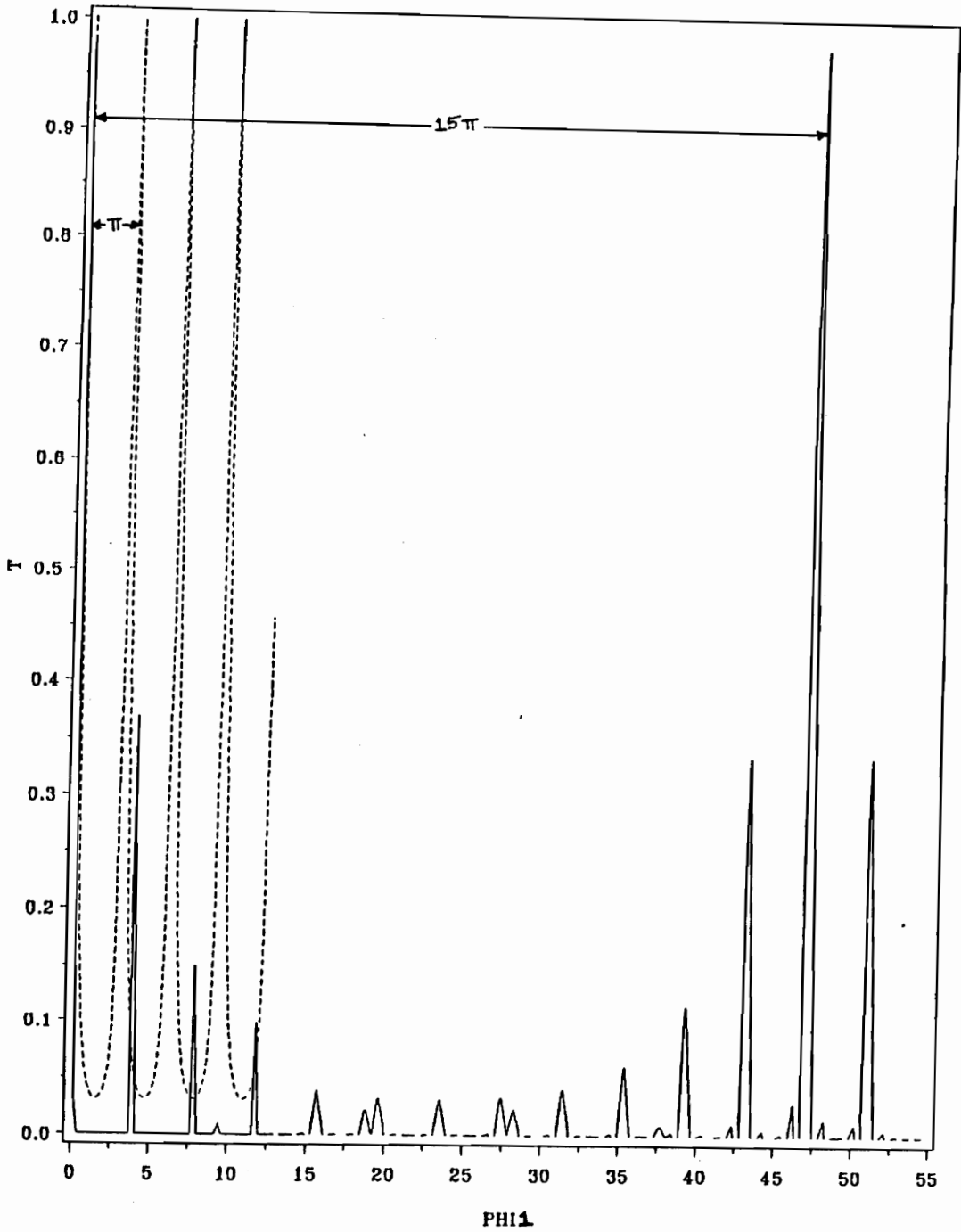


Figure 8 : Improvement in Tuning range in a 4-Mirror F-P : $R_1 = R_4 = 0.7$, $R_2 = R_3 = R_{2,c} = 0.9842$, $FSR_2 = (5/4).FSR_1$ and $FSR_3 = (3/2).FSR_1$. The improvement is fifteenfold. The solid and dashed curves correspond to the 4 and 2 mirror filters respectively.

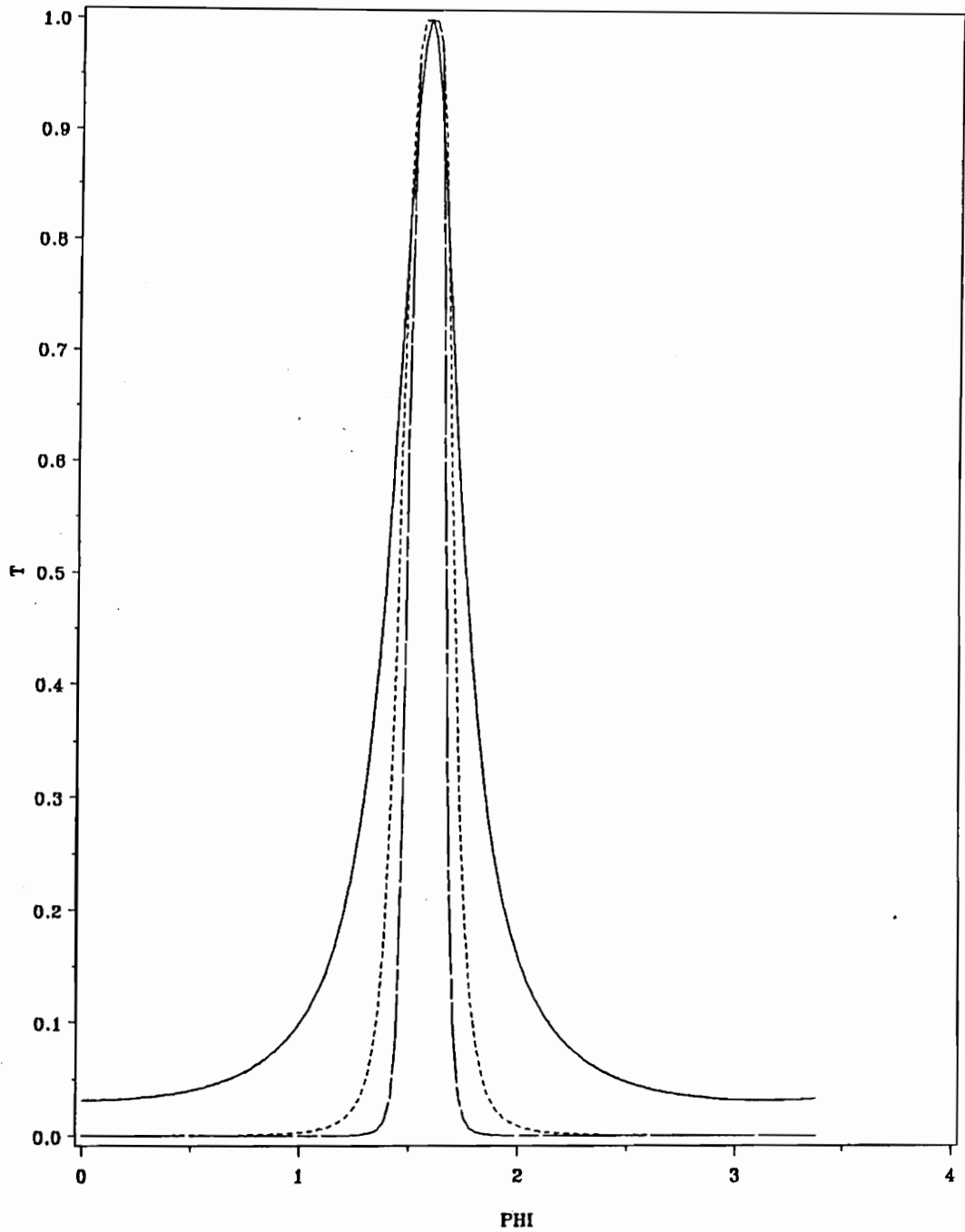


Figure 9 : Transmission Spectra of two and multimirror F-P filters : The solid, dotted and dashed curves correspond to the 2, 3 and 4 mirror F-P filters respectively.

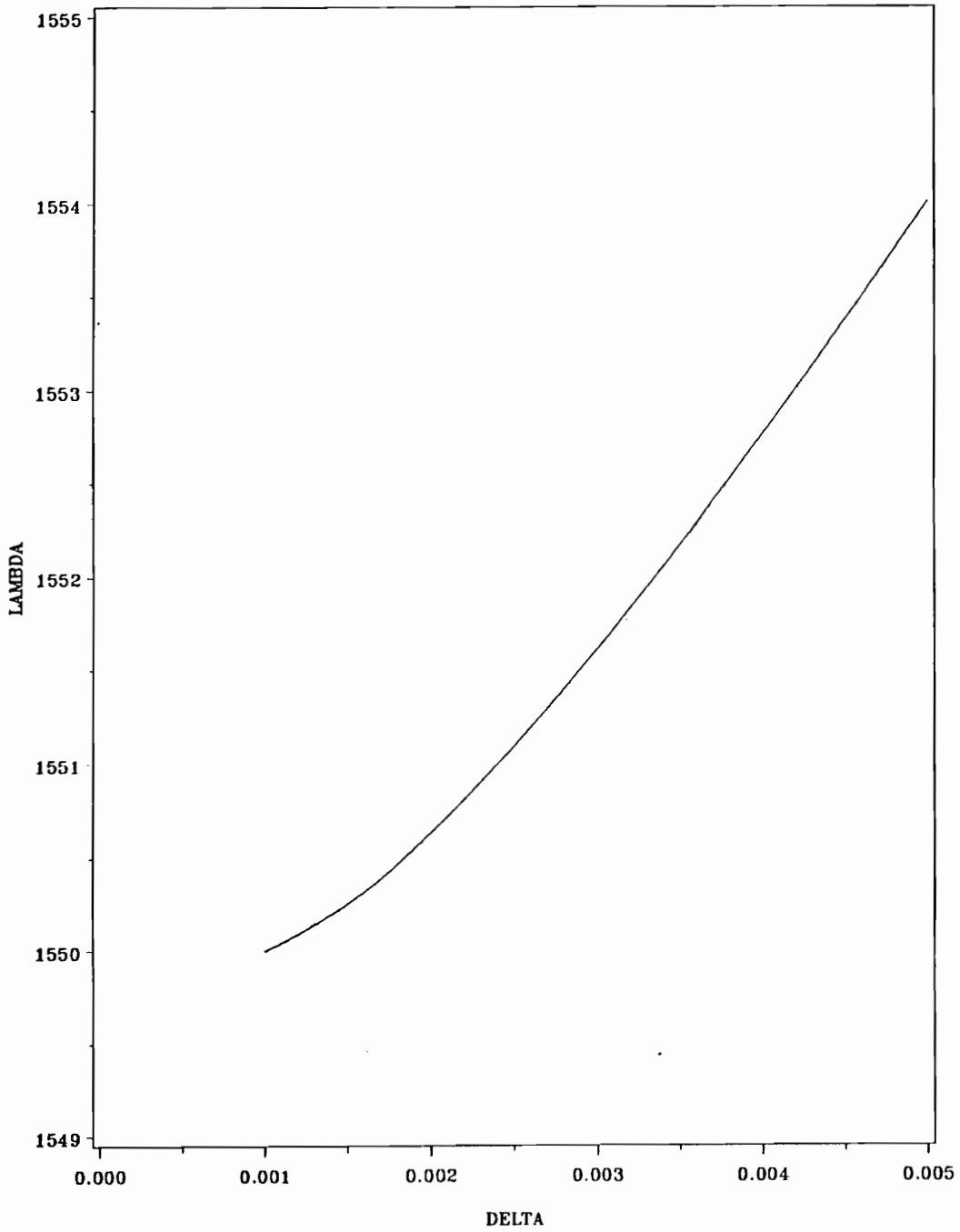


Figure 10 : Resonant wavelength variation with Δ : Δ is varied between 0.001 and 0.005 to ensure that $V < 2.405$. The core index is $n_1 = 1.48$ and core radius is $a = 4 \mu\text{m}$.

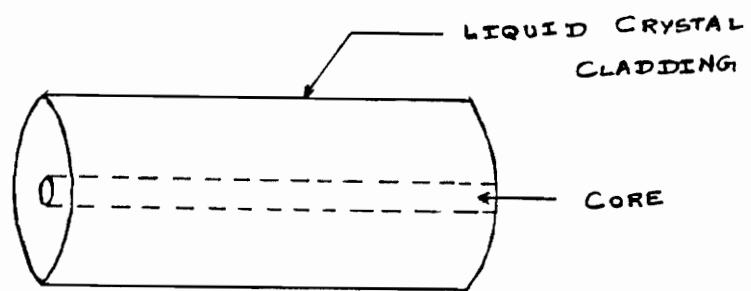


Figure 11 : Geometry of the filter : The filter has a glass core and a Liquid Crystal cladding.

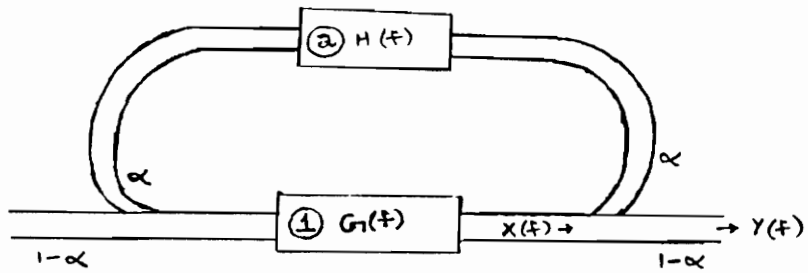


Figure 12 : The F-P filter with optical feedback : α is the tap ratio of both the couplers. $X(f)$ is the normalized output power of cavity 1. Also, $Y(f)$ is the normalized output power of the filter (i.e., on the output side of the directional coupler on the right).

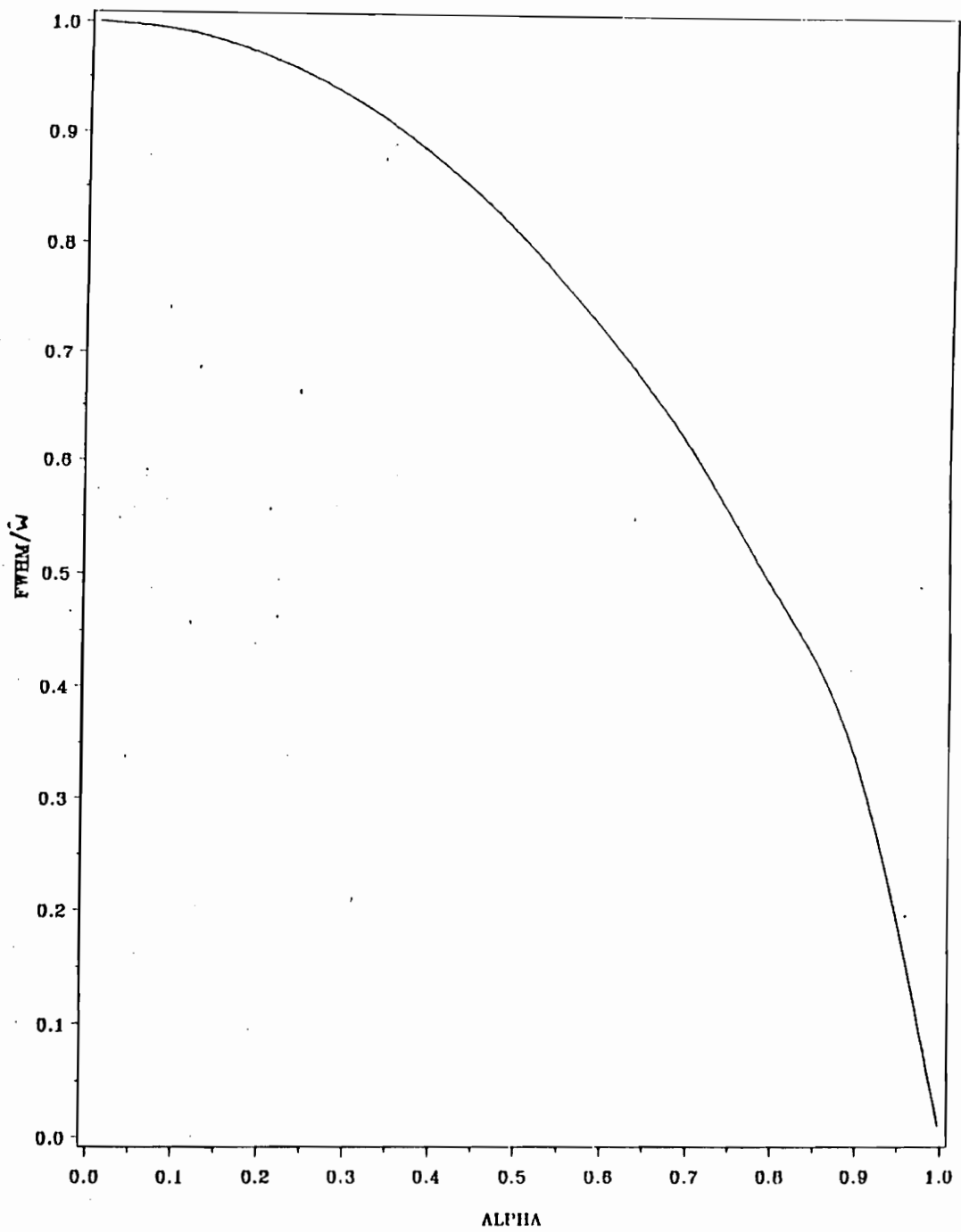


Figure 13 : FWHM bandwidth vs. Tap ratio α : Note that as tap ratio α increases, FWHM BW of the filter decreases.

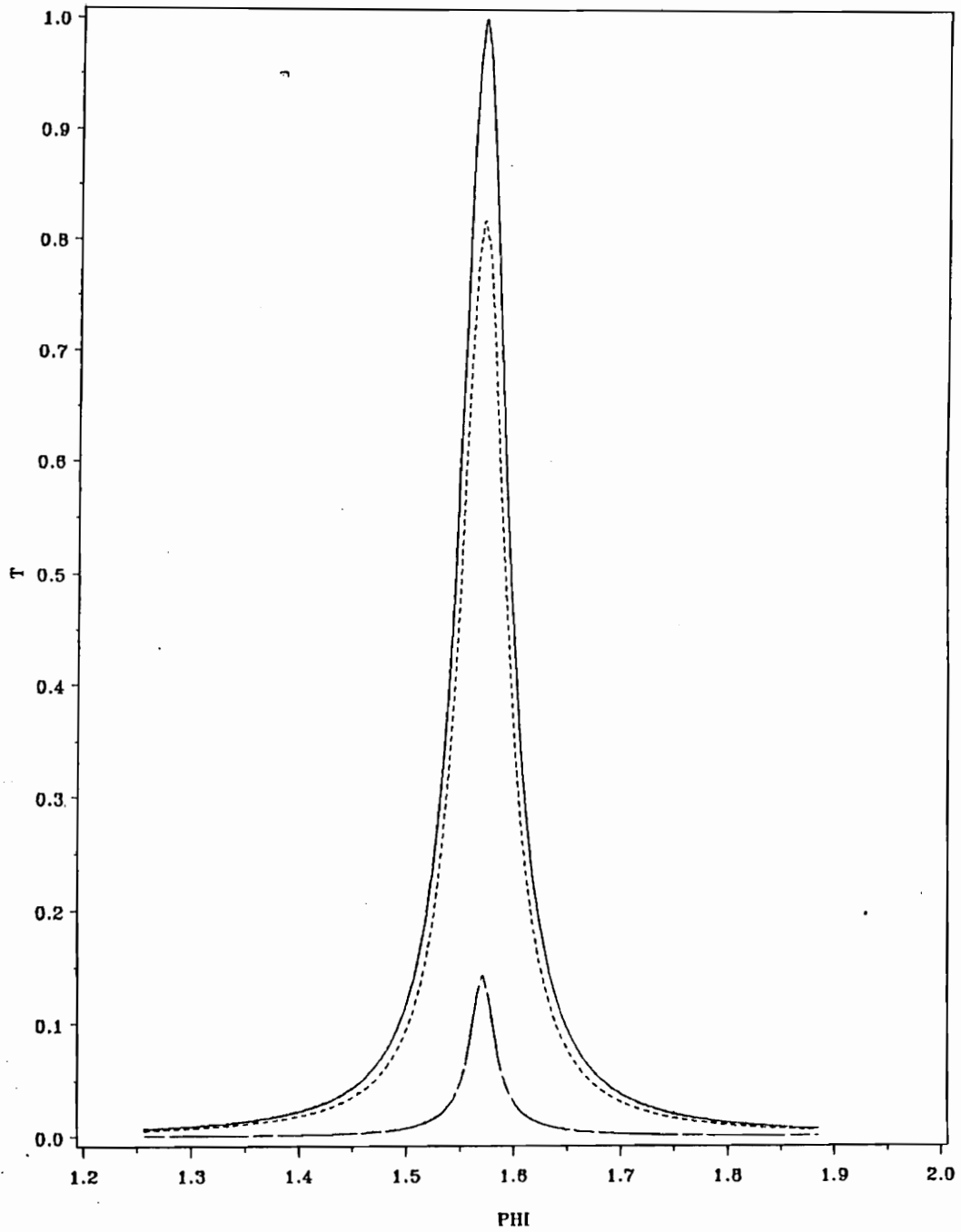


Figure 14 : **Transmission Spectrum of the Feedback filter** : Two different tap ratios have been considered. Note the decrease in bandwidth with respect to that of a single cavity F-P filter. The solid, dotted and dashed curves correspond to the single cavity filter and feedback filter with $\alpha = 0.1$ and 0.75 respectively.

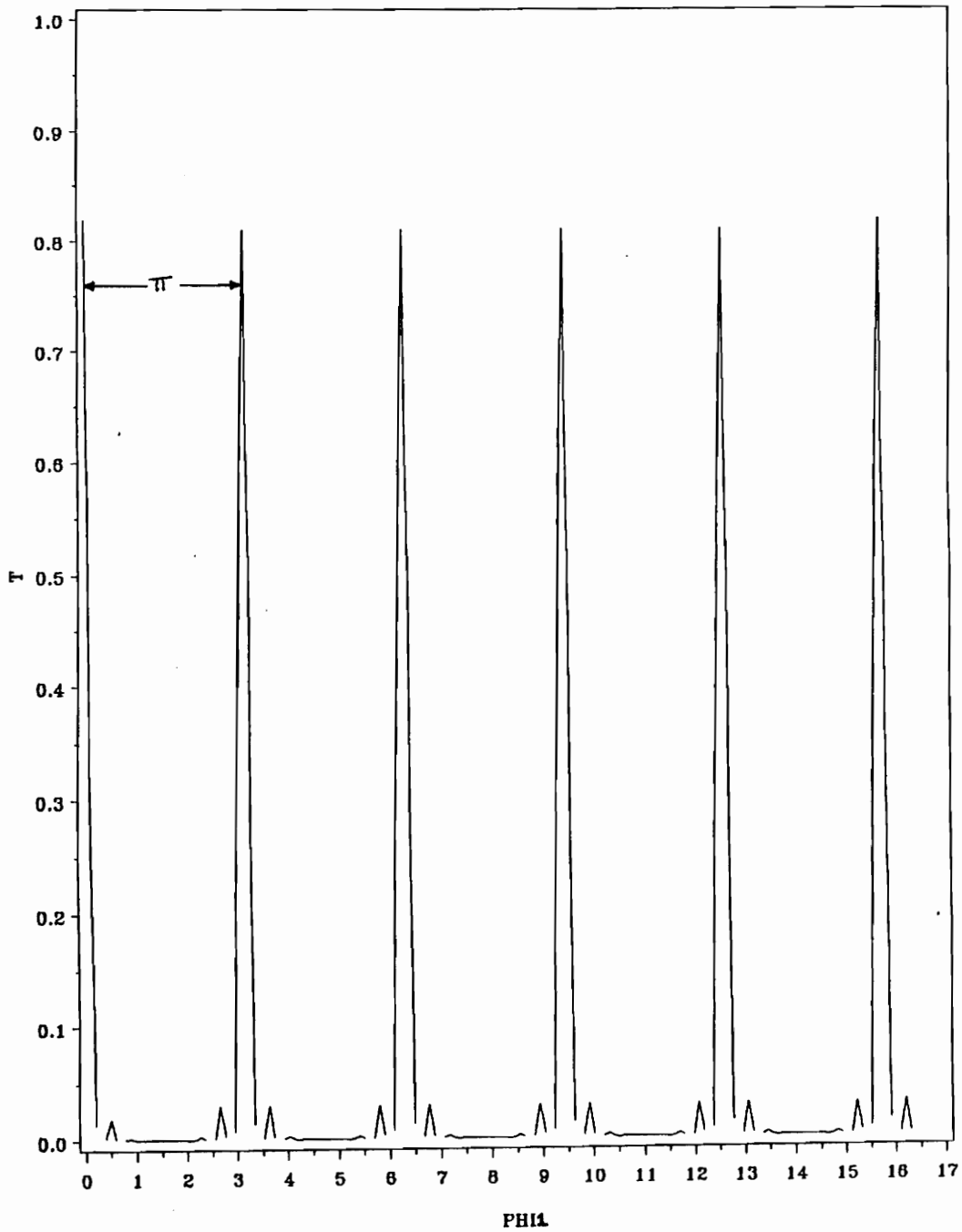


Figure 15 : Loss of tuning range improvement in the Feedback filter : A low value of tap ratio has been chosen namely $\alpha = 0.1$. Also, $FSR_2 = (5/4).FSR_1$, $R_1 = R_2 = 0.95$.

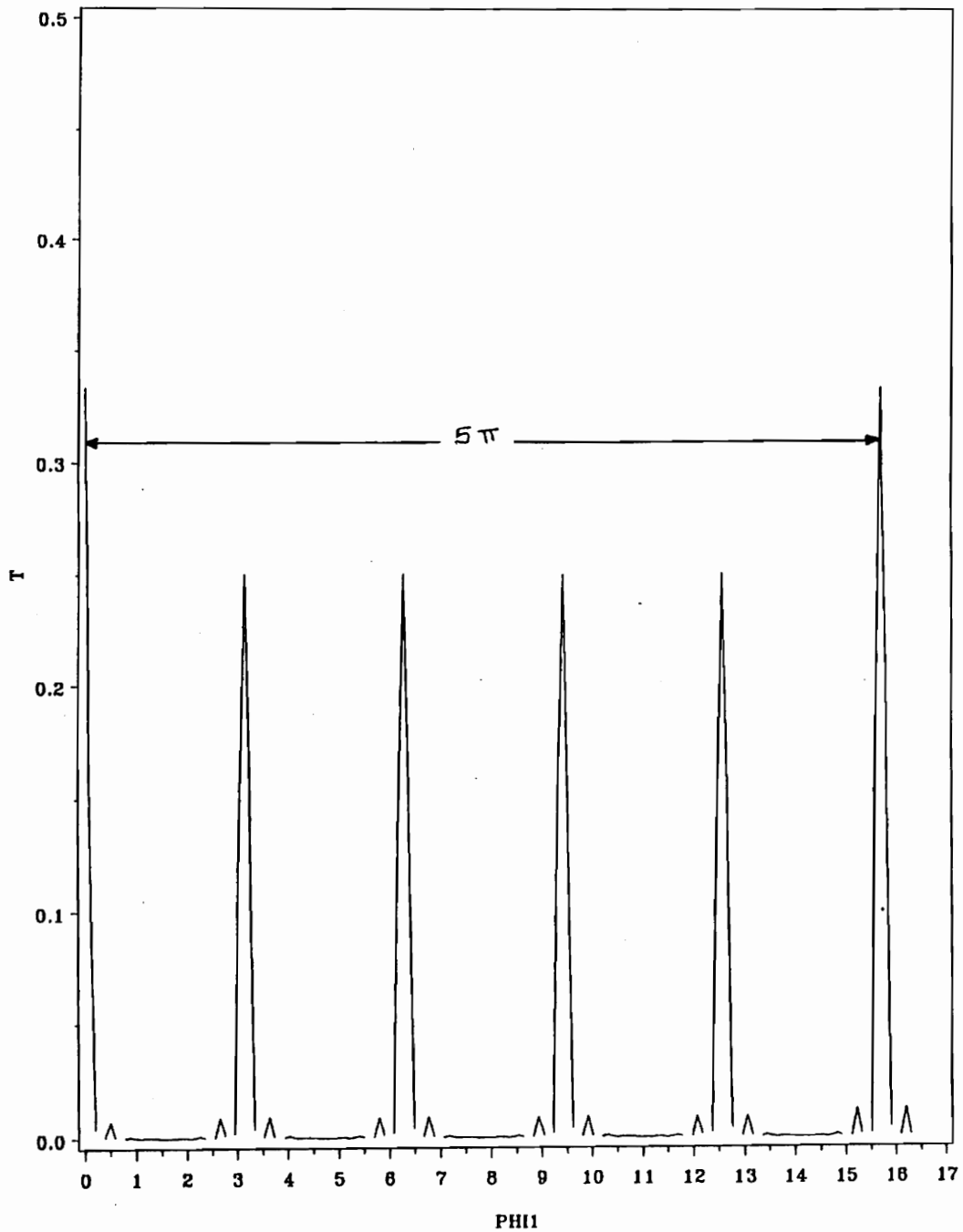


Figure 16 : Improvement in tuning range in the Feedback filter : A moderately high value of tap ratio has been chosen namely $\alpha = 0.5$. Also, $FSR_2 = (5/4).FSR_1$, $R_1 = R_2 = 0.95$.

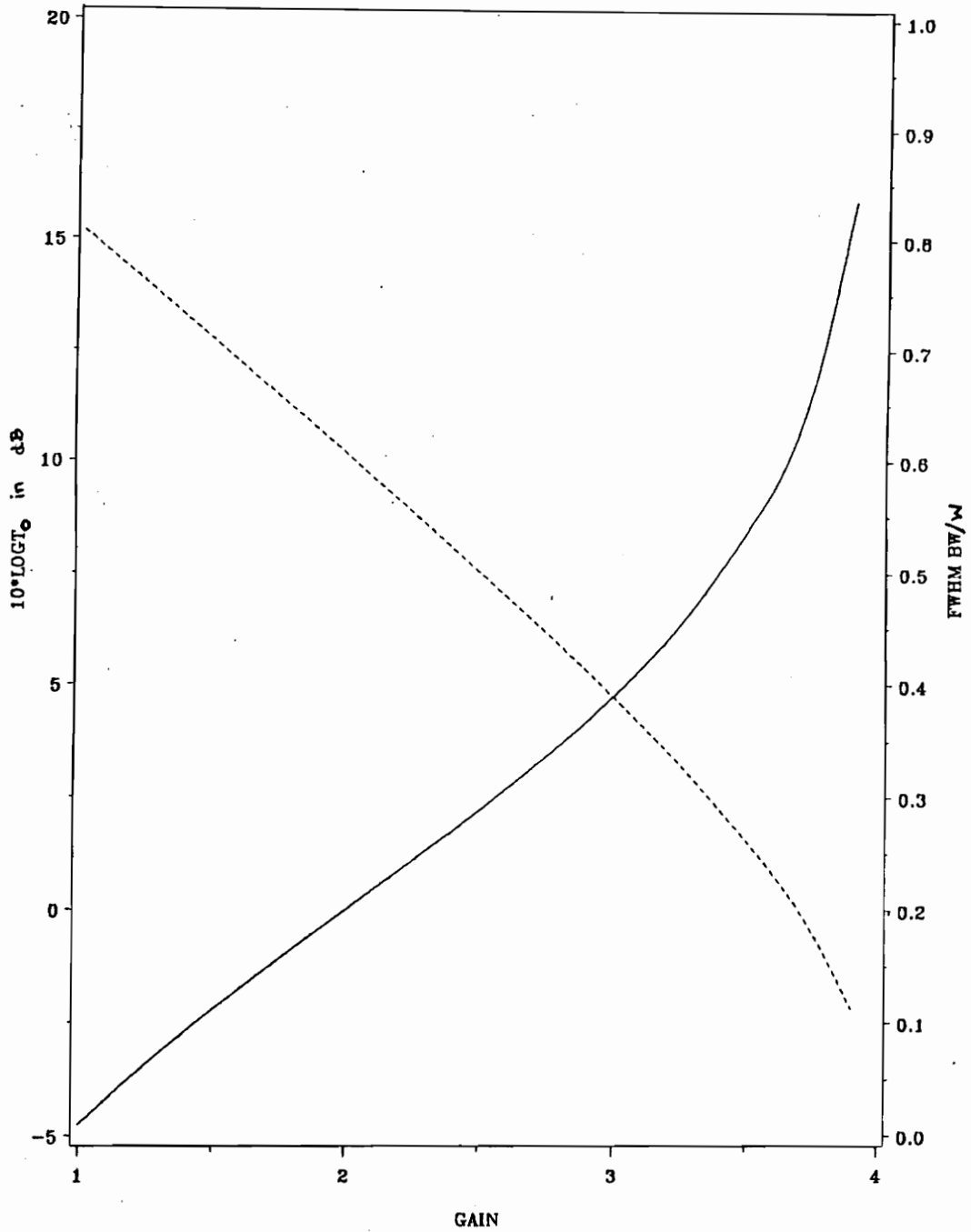


Figure 17 : Dependence of Peak transmission and FWHM BW on amplifier gain : The tap ratio is $\alpha = 1/2$. The solid and dashed curves represent the peak transmission in dB and the FWHM BW in terms of the bandwidth of a single cavity respectively.

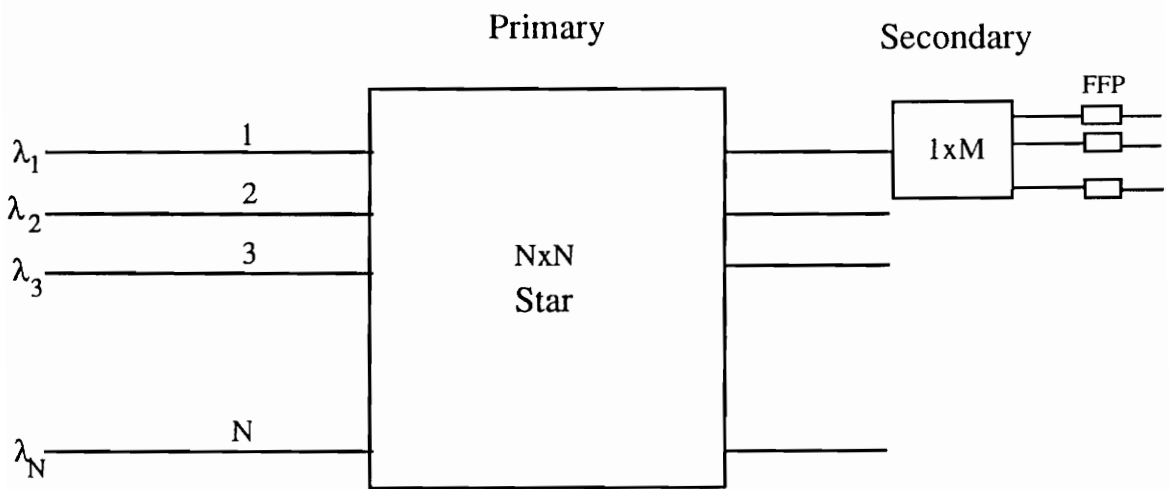
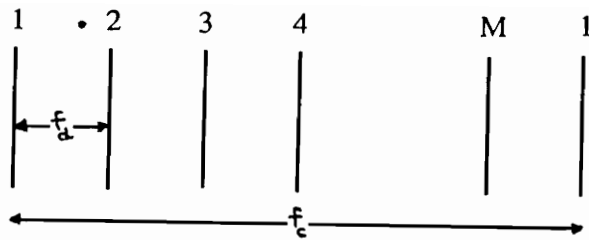
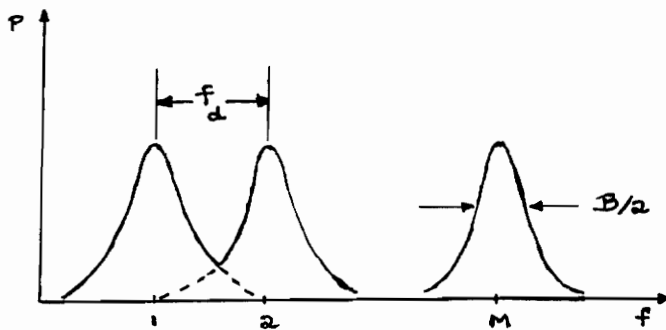


Figure 18 : The FDMA M-ary FSK Star Network : The network has N nodes.



(a)



(b)

Figure 19a : **M-ary signal set** : f_d is the frequency deviation between adjacent component signals of the signal set and f_c is the channel spacing.

Figure 19b : **Continuous phase M-ary FSK power spectrum** : Note the M peaks separated by f_d and of width $B/2$ each. Power in each peak is P/M where P is the total power in the channel.

9.0 References

1. M. Born and E. Wolf, "Principles of Optics", New York: Macmillan, 1959, pp. 325 - 329.
2. J. Stone and D. Marcuse, "Ultrahigh Finesse Fiber Fabry-Perot Interferometers", Journal of Lightwave Technology, vol. LT - 4, No. 4, pp. 382 - 385, April 1986.
3. J. Stone and L.W. Stulz, "Pigtailed High-Finesse Tunable Fiber Fabry-Perot Interferometers with large, medium and small Free Spectral Ranges", Electronics Letters, vol. 23, pp. 781 - 783, 1987.
4. H. Ishio et al, "Review and Status of Wavelength-Division-Multiplexing Technology and Its Application", Journal of Lightwave Technology, vol. LT - 2, No. 4, pp. 448 - 463, August 1984.
5. M. Young, "Optics and Lasers", Springer-Verlag, 1986.
6. S.S. Wagner and H. Kobrinski, "WDM Applications in Broadband Telecommunication Networks", IEEE Communications Magazine, pp. 22 - 30, March 1989.
7. W.V. Sorin et al, "Tunable Single-mode Fiber Reflective Grating Filter", Journal of Lightwave Technology, vol. LT - 5, No. 9, pp. 1199 - 1202, September 1987.

8. R. Zengerle and O.G. Leminger, "Wavelength-Selective Directional Coupler made of Nonidentical Single-mode Fibers," *Journal of Lightwave Technology*, vol. LT - 4, No. 7, pp. 823 - 826, July 1986.
9. R. Zengerle and O.G. Leminger, "Narrowband Wavelength-Selective Directional Couplers made of Dissimilar Single-mode Fibers", *Journal of Lightwave Technology*, vol. LT - 5, No. 9, pp. 1196 - 1198, September 1987.
10. A.A.M. Saleh and J.Stone, "Two-Stage Fabry-Perot Filters as Demultiplexers in Optical FDMA LAN's", *Journal of Lightwave Technology*, vol. 7, No. 2, pp. 323 - 330, February 1989.
11. H. van de Stadt and J.M. Muller, "Multimirror Fabry-Perot interferometers", *Journal of Optical Society of America*, vol. 2, No. 8, pp. 1363 - 1370, August 1985.
12. W.B. Jones, "Introduction to Optical Fiber Communication Systems", New York: Holt, Reinhart and Winston, pp. 80 - 90, 1988.
13. C. Hu and J.R. Whinnery, "Field-Realigned Nematic-Liquid-Crystal Optical Waveguides", *IEEE Journal of Quantum Electronics*, vol. QE-10, No. 7, pp. 556 - 562, July 1974.
14. I.P. Kaminow et al, "FDMA-FSK Star Network with a Tunable Optical Filter Demultiplexer", *Journal of Lightwave Technology*, vol. 6, No. 9, pp. 1406 - 1414, September 1988.
15. S. Murata et al, "Frequency Modulation and Spectral Characteristics for a 1.5 μm Phase-Tunable DFB Laser", *Electronics Letters*, vol. 23, pp. 12 -14, 1987.
16. R.W. Lucky, J. Salz and E.J. Weldon Jr., "Principles of Data Communications", New York: McGraw-Hill, 1968.

17. G. Ungerboeck, "Trellis-Coded Modulation with Redundant Signal Sets Part I:Introduction", IEEE Communications Magazine, pp. 5-11, February 1987.
18. P.Z. Peebles Jr., " Digital Communication Systems," Prentice Hall, 1987.
19. P.S. Henry, "Error-rate Performance of Optical Amplifiers", OFC, vol. 5, Houston, Texas, pg. 170, 1989.
20. P.S. Henry et al, "Introduction to Lightwave Systems" in *Optical Fiber Telecommunications II*, ed. by S.E. Miller and I.P. Kaminow, Academic Press, 1988, Chapter 21.
21. M.S. Goodman, "Multiwavelength Networks and New Approaches to Packet Switching", IEEE Communications Magazine, pp. 27 - 35, October 1989.
22. M.S. Goodman et al, "Application of Wavelength Division Multiplexing to Communication Network Architectures", ICC, vol. 2, Toronto, Canada, pp. 931 - 934, 1986.
23. R.M. Bulley et al, "Design and Demonstration of the LAMBDANET TM System : A Multiwavelength Optical Network", IEEE/IEICE Global Telecom. Conf., pp. 37.4.1 - 37.4.4, 1987.
24. K.Y. Eng, "A Photonic Knockout Switch for High-Speed Packet Networks", IEEE/IEICE Global Telecom. Conf., pp. 47.2.1 - 47.2.5, 1987.
25. Y.S. Yeh et al, "The Knockout Switch : A Simple, Modular Architecture for High-Performance Packet Switching", IEEE Journal of Selected Areas in Communications, vol. SAC-5, pp. 1274-1283, October 1987.
26. A.S. Acampora, "A Multichannel Multihop Local Lightwave Network", Proc. Globecom., pp. 1459-1467, 1987.

27. A.S. Acampora et al, "Multihop Lightwave Networks : A New Approach to Achieve Terabit Capabilities", Proc. ICC '88, vol. 1, pp. 1478-1484, 1988.
28. S. Suzuki et al, "A Phoyonic Wavelength-Division Switching System Using Tunable Laser Diode Filters", Journal of Lightwave Technology, vol. 8, No. 5, pp. 660 - 666, May 1990.

Vita

B.S. Srinivas was born in Bangalore, India on November 1, 1966. He received his B.Tech in Electrical Engineering from the Indian Institute of Technology, Bombay in May 1988. He then joined Virginia Tech in August 1988 for an M.S. His research interests are optical fiber communications and communication network performance analysis. Currently twenty three, he plans to go ahead for a Ph.D. in Electrical Engineering.